The zircon story of the Pearl River (China) from Cretaceous to present

Jie He[a,b,c], Eduardo Garzanti[c,*], Licheng Cao[b,d], Hua Wang[a,b,*]

[a] *School of Earth Resources, China University of Geosciences, Wuhan 430074, China*

[b] *Key Laboratory of Tectonics and Petroleum Resources, China University of Geosciences, Wuhan 430074, China*

[c] *Laboratory for Provenance Studies, Department of Earth and Environmental Sciences, University of Milano-Bicocca, Milano 20216, Italy*

[d] *College of Marine Science and Technology, China University of Geosciences, Wuhan 430074, China*

Email addresses: jiehe19920402@163.com, eduardo.garzanti@unimib.it, licheng.cao@gmail.com, wanghua@cug.edu.cn

Corresponding author: Eduardo Garzanti (eduardo.garzanti@unimib.it); Hua Wang (wanghua@cug.edu.cn)

Keywords: *Sediment provenance; Detrital zircon geochronology; Paleotopographic reconstructions; Tibetan Plateau; Pearl River and Pearl River Basin; South China Sea.*

ABSTRACT

The modern Pearl River originates from SE Tibet and debouches into the South China Sea. The development of the Pearl River is closely related to the evolving topography following the tectonic evolution of the southern China continental margin from subduction of the paleo-Pacific Ocean in the Cretaceous to Cenozoic rifting linked with the opening of the South China Sea and uplift of Tibet caused by the India-Eurasia collision. How topographic changes affected the development of the Pearl River, however, is still unclear. Here we use original and literature data on detrital zircon ages from both modern Pearl River sands and ancient sediments drilled in offshore basins to reconstruct the evolution of the paleo-Pearl River catchment through time. Six phases are identified: 1) Early Cretaceous: the paleo-Pacific plate was subducting beneath the South China block and topography in South China was tilted to the west. The paleo-Dong River began to develop with limited length. 2) Late Cretaceous: back-arc extension in the South China Sea contributed further to the west-tilted topography. The paleo-Bei River started to develop and the paleo-Dong River continued to expand across southeasternmost China. 3) Paleocene to Eocene: active rifting in the South China Sea induced a major topographic change. The paleo-Dong and paleo-Bei joined, forming the paleo-Lower Xi River. 4) Early Oligocene: active uplift of Tibet and onset of sea-floor spreading in the South China Sea led to subsidence in of the Cathaysia Block. The paleo-Dong, paleo-Bei, and paleo-Lower Xi rivers remained limited to eastern Cathaysia. 5) Late Oligocene: accelerated uplift of eastern Tibet and post-rift subsidence of the northern South China Sea margin induced a radical change in the landscape of southern China, and transition from west-tilting to east-tilting topography. The paleo-Pearl River started to incorporate also its present western branches. 6) Early to middle Miocene: the east-tilting topography was enhanced during rapid uplift of Tibet and progressive closure of the proto-South China Sea, while the Pearl River evolved to its present configuration.

1. INTRODUCTION

Many different methods have been used to investigate geological evolution and sediment-generation processes in big river drainages all over the world (e.g., Gaillardet et al., 1999; von Blanckenburg, 2005; Borges et al., 2008; Hinderer, 2012; Clift, 2015). The compositional and geochronological signatures of bulk sediment have proved to be an excellent tool to trace erosion patterns in space and time during progressive unroofing of source rocks (Garzanti, 2016; Resentini et al., 2018). Zircon is a durable mineral which is largely preserved after chemical attack during subsequent stages of the sedimentary cycle (Morton and Hallsworth, 2007; Garzanti, 2017), and consequently detrital zircon U-Pb age distributions have been widely used to provide provenance information on modern and ancient sediments (e.g., Cawood et al., 2003; Clift, 2016; Xu et al., 2017; Garzanti et al., 2016, 2018; Lei et al., 2019).

The Pearl River originates from SE Tibet and deposits its sediment load into the South China Sea after receiving several main tributaries (Hongshui, Liu, Yu, Gui, He, Bei and Dong rivers; Fig. 1). In this large river catchment, we have investigated how tectonic and climatic changes have controlled topography, sediment generation and sediment composition from the Early Cretaceous to the present time (Shao et al., 2016; Liu et al., 2017; Cao et al., 2018).

Unlike other major rivers such as the Yangtze, the Yellow River, and the Red River (Clark et al., 2004; Clift et al., 2006b; Stevens et al., 2013; Zheng et al., 2013; Vezzoli et al., 2016), which originate from the gently tilted, low-relief, high-elevation surface of SE Tibet in southeast Asia, the drainage network of the Pearl River is thought to have initiated from the South China margin and to have subsequently progressed westward by headward erosion across the continental interior and into the margin of the SE Yunnan plateau (Clift et al., 2002; Clark et al., 2004; Shao et al., 2008a, 2015, 2017; Liu et al., 2017; Cao et al., 2018). Several different methods have been used to trace sediment provenance and erosion patterns in the Pearl River catchment, including landscape morphometry, bulk-sediment geochemistry, heavy-mineral analyses, detrital-zircon geochronology, and Nd and Sr isotope geochemistry (Xiang et al., 2011; Zhao et al., 2015; Shao et al., 2016; Liu et al., 2017; Cao et al., 2018). Xiang et al. (2011) studied heavy minerals in modern Pearl River sediments and identified three distinctive assemblages characterizing the Upper Xi River, the

Lower Xi River, and the Bei and Dong rivers. Zhao et al. (2015) carried out U-Pb dating of detrital zircons in all main branches of the modern Pearl River and distinguished eight main age clusters: 2800-2300 Ma, 2000-1800 Ma, 1100-700 Ma, 600-400 Ma, 380-230 Ma, 200-80 Ma, and < 65 Ma. Liu et al. (2017) estimated the sediment contribution from different tributaries by detrital-zircon U-Pb dating coupled with bulk-sediment geochemistry and Nd and Sr isotopes, and concluded that the Pearl River expanded westwards to reach its modern configuration not before the end of the Oligocene (23 Ma). Based on the zircon record from the northern South China Sea, Cao et al. (2018) documented a major provenance change that took place in response to progressive expansion of the river network from a small coastal river in the early Oligocene to a near-modern configuration in the early Miocene, in connection with uplift of SE Tibet.

Tectonic events have a direct and profound impact on the topography of a region, causing the fluvial network to reorganize accordingly (e.g., Castelltort et al., 2012; Zhang et al., 2019). Because during its entire history the Pearl River has been closely connected both to the uplift of SE Tibet and to the evolution of the South China Sea (Shao et al., 2008a, 2016; Cao et al., 2018), the tectonic and topographic changes that occurred in SE Tibet and in the South China Sea need to be taken into full account when discussing the evolution of the paleo-Pearl River. On the basis of the study of river incision based on low-temperature thermochronology (e.g. Yang et al., 2016; Zheng et al., 2013), and of geomorphological studies based on stable isotopes (e.g. Hoke et al., 2014; Li et al., 2015), SE Tibet was estimated to have attained its high elevation either in the Paleocene-Eocene or in the middle-late Miocene. In the South China Sea area, a major change took place in the Late Cretaceous, from subduction of the paleo-Pacific plate to Cenozoic rifting culminated of the South China Sea at Paleocene-Eocene times (Charvet et al., 1994; Lapierre et al., 1997; Shu and Zhou, 2002; Cullen et al., 2010; Li et al., 2012; Morley, 2016; Sun, 2016; Ye et al., 2018). Because the wide regional tectonic framework has been taken into account only partially in previous reconstructions, many aspects of the paleo-Pearl River drainage basin have remained poorly understood. Further comprehensive studies are thus required to evaluate tectonic and climatic control on topographic changes and erosion patterns.

In this study, we present original U-Pb age data on detrital zircons from eight modern sands from major Pearl River tributaries, from one modern marine sand from the Qinzhou Bay, and from four sandstones

cored in the northern South China Sea (Figs. 1 and 2). Modern river-sand samples are complementary to those used in previous detrital-geochronology studies, which mainly focused on the central and eastern parts of the catchment. The upper Oligocene sample W9 was cored in the western part of the Pearl River Mouth Basin, complementary to previously studied cores located in its central and eastern parts. Samples W10, W11, and W12, ranging in age from Eocene to early Oligocene, are from three different sites in the Beibuwan Basin (Fig. 3), the only basin in the north South China Sea where geochonological studies had not been carried out previously. We have included data from the Beibuwan Basin, which is located to the east of the Red River mouth, because it may have been fed from paleo-Pearl River sediments in the past (Van Hoang et al., 2009). Our principal aim is to reconstruct the evolution of the Pearl River and to identify how such a large fluvial network has recorded, and has reacted to the regional tectonic and climatic events that have controlled landscape changes from the Early Cretaceous to the present time.

2. GEOLOGICAL BACKGROUND

2.1. Pearl River

The Pearl River (Chinese name Zhu Jiang, where *zhu* = pearl and *jiang* = river; length 2320 km, catchment area 4.5×10^5 km^2) is the third longest river in China after the Yangtze (Changjiang) and the Yellow River (Huanghe). Main tributaries are the Xi (west), Bei (north), Dong (east) rivers that join into the Pearl River Delta (Fig.2). The westernmost branches, the Nanpan and Beipan rivers (*nan* = south, *bei* = north), are sourced in the Yunnan-Guizhou Plateau of SE Tibet at elevations up to 2800 m a.s.l. and flow eastward across the Yangtze Block where elevation is > 1000 m. Downstream, the river flows across the Cathaysia block, where it takes the name of Xi River after confluence with the Liu, Yu, Gui, and He tributaries. The Xi River joined by the Bei and Dong tributaries upstream of the delta, eventually debouches into the northern South China Sea (Fig. 1).

The Pearl River catchment, situated at tropical latitudes, is strongly influenced by the East Asia Summer Monsoon. The average annual temperature ranges from 14 to 22^{0}C, with extreme values up to 42 ^{0}C and down to -10 ^{0}C. Mean precipitation is 1.5 m and decreases markedly westward, with a maximum of 2.4 m in

the southeast and a minimum of 0.7 m in the northwest (Q. Zhang et al., 2012; Liu et al., 2015). The wet season, spanning from April to September, accounts for nearly 80 % of the total annual precipitation.

Most of the Pearl River's sediment load accumulates on the SE China continental margin and in the Pearl River Mouth Basin offshore. Sediment is derived from rocks of the Yangtze Craton exposed in the north and northwest, largely consisting of upper Paleozoic carbonates and Triassic dolostones and continental siliciclastic red beds (Chen et al., 1993; Hu et al., 2013), and rocks of the Cathaysia Block in the southeast, where largely granites and locally volcanic rocks are exposed (Jahn et al., 1990; Hu et al., 2013) (Fig. 2). The Yangtze and Cathaysia blocks collided to form the South China Block at 800-1000 Ma (Wang et al., 2007). This composite terrane includes (Fig. 2): a) the Chuandian fragment (ca. 775 Ma) (Fig. 4E), and b) the Permian Emeishan continental-flood basalts (ca. 260 Ma) (Fig. 4C), exposed in the northwestern corner of the Pearl River catchment; c) the Jiangnan orogen in the north, including mainly Precambrian basement in its western part, with most zircons yielding ages around 820 Ma and subordinately Mesozoic and Paleoproterozoic ages (Fig 4F); d) the North Vietnam terrane exposed in the southwestern corner of the catchment, and yielding zircon ages clustering at ca. 80 Ma, 240 Ma, and 1600-3200 Ma (Fig. 4H); and e) the Yunkai Massif in the south, including Precambrian basement (ca. 940 Ma), latest Ordovician to Silurian granites (420-450 Ma), and Indosinian granites (ca. 250 Ma) (Fig. 4G).

Because it drains mainly Yanshanian (ca. 170 Ma) (Fig. 4A), Indosinian (ca. 230 Ma) (Fig. 4B), Silurian (ca. 425 Ma) (Fig. 4D) granites, as well as Proterozoic basement rocks, the Pearl River is characterized by a multimodal zircon-age distribution characterized by main 230-245 Ma, 400-450 Ma, and 750-850 Ma age clusters with additional younger (Cretaceous to Jurassic) and older (Paleoproterozoic to Neoarchean) ages (Fig. 4). The Beipan and Nanpan rivers have their headwaters into the Emeishan Large Igneous Province and in the Chuandian fragment, and mainly drain the northwestern part of the Youjiang Basin where Triassic deep-sea turbidites and Paleozoic carbonates are extensively exposed (Fig. 2). They join downstream to form the Hongshui River, which flows through the eastern part of the Youjiang Basin together with the northern You branch of the Yu River, whereas its southern Zuo branch is sourced in North Vietnam. The Liu, Gui, and He rivers drain the western part of the Jiangnan orogen, which is a Neoproterozoic accretionary belt issued from the Yangtze-Cathaysia collision (Chu et al., 2012; Lehrmann et al., 2015). The Bei and Dong

rivers flow southward across the eastern part of the Cathaysia Block, largely consisting of Yanshanian granites (Fig. 2).

2.2. South China Sea and Pearl River Mouth Basin

Southern China evolved from a convergent plate boundary associated with subduction of the paleo-Pacific plate to a divergent one in the Late Cretaceous, followed by rifting in the Paleocene and opening of the South China Sea in the Oligocene (Morley, 2016; Ye et al., 2018). Geochemical fingerprints of igneous rocks confirm this Late Cretaceous transition from an earlier Andean-type margin to a Western Pacific-type margin, as a response to slab roll-back and increase of subduction angle (Zhou and Li, 2000; Shu and Zhou, 2002; Li et al., 2012; He and Xu, 2012; Shao et al., 2017a; Ye et al., 2018). During the late Paleocene to Eocene, regional extension led to the formation of rifts, including the Pearl River Mouth Basin in the northern South China Sea (Morley, 2016). Intense tectonic and volcanic activity prevented the development of a large unconfined river system in southern China at that time (Cao et al., 2018). Wang (2004) suggested that topography in continental China was generally tilted towards the west during the Mesozoic, when the main rivers were sourced in eastern China and flowed westward. The landscape was thus radically different from the pronounced eastward slopes of the present day, which are the consequence of Paleocene collision between India and Asia (Hu et al., 2016) and consequently enhanced uplift of SE Tibet. Based on newly acquired 3D seismic reflection and industrial well data, Ye et al. (2018) recently proposed a multiphase model for the tectonic evolution of the South China Sea area in the Late Cretaceous.

The Pearl River Mouth Basin (Fig. 2) started to open by extension along the northern margin of the South China Sea since the close of the Cretaceous, as documented by well-developed, fault-bounded asymmetric grabens and half-grabens in its northern part (Huang et al., 2003; Liu et al., 2016). Fluvial volcaniclastic sediments were deposited during the Paleogene (56-30 Ma) syn-rift stage. Following initiation of sea-floor spreading in the South China Sea (C. Li et al., 2014), the post-rift stage (30 Ma to present) was characterized by transition to deltaic, carbonate-platform, and deep-sea sediments deposited in the Neogene (Liu et al., 2016).

2.3. Tibetan Plateau uplift

The uplift history of the Tibetan Plateau, which displays the most elevated topography on Earth, began as early as the mid-Cretaceous (Murphy et al., 1997; Wang et al., 2017; Lai et al., 2019) and accelerated after ca. 60 Ma, when India collided with Asia along the Yarlung-Zangbo suture zone (DeCelles et al., 2014; Hu et al., 2016). Recent modelling of global circulation suggested that the Tibetan Plateau may have reached only low to moderate (< 3000 m) elevations during the Eocene (Botsyun et al., 2019). Low-temperature thermochronometric studies identified four stages of Cenozoic uplift, at 60-35 Ma, 25-17 Ma, 12-8 Ma, and ~5 Ma (G. Wang et al., 2011). Wang et al (2008) suggested that rapid uplift occurred earlier in central Tibet (around 40 Ma) than in southern Tibet. Dupont-Nivet et al. (2008) constrained the main phase of uplift as 38 Ma, based on pollen analysis in the Xining Basin. Clift et al. (2006a) concluded that surface uplift in eastern Tibet and southwest China should have begun no later than 24 Ma based on the Nd isotope signature of sediments in the Hanoi Basin (Vietnam). Thermochronological data indicated that rapid uplift and exhumation of the eastern Tibet Plateau, associated with strike-slip faulting and thrusting, took place at 20-16 Ma and ~5 Ma (Lai et al., 2007).

3. LITERATURE DATA ON ZIRCON AGES FROM OFFSHORE BASINS

The Pearl River Mouth Basin contains a continuous sedimentary archive, and detrital-zircon U-Pb geochronology has been carried out extensively on several industrial wells (sites H9, L35, L18, L21, and L13) and on IODP (International Ocean Discovery Program) cores at Site U1345, located near the continent-ocean transition zone in the northern South China Sea (Figs. 2 and 3), to obtain information on the erosional evolution of the Pearl River (Xu et al., 2007, 2016; Zhao et al., 2015; Shao et al., 2016, 2017; Zhong et al., 2017; Cao et al., 2018). Zircon-age spectra from Eocene rocks cored at IODP Site U1435 are unimodal with peak at ca. 120 Ma (Fig. 5A). Similar U-Pb ages have been reported for detrital zircons in Palawan and Borneo, at the southern margin of the South China Sea (Walia et al., 2012; Suggate et al., 2014), but fluvial connection between these now widely separated area was unlikely because rifting was well underway at this stage (Shao et al., 2017b).

U-Pb zircon-age spectra from Lower Cretaceous to middle Miocene rocks cored in industrial wells H9, X28, L35, L18, L21, and L13 (Fig. 2) invariably show a major cluster at 100-200 Ma (Fig. 5). This young peak invariably dominates the unimodal zircon-age spectra in Lower Cretaceous, Upper Cretaceous, and Eocene-Oligocene strata from IODP Site U1345 and wells L35, L18, and L21. Such a simple age distribution and the typical euhedral to elongate shape of zircon grains imply a nearby source (Shao et al., 2016). Provenance from the Dongsha Islands, lying close to sample L18, has been suggested for these samples by Liu et al. (2011). Lower and upper Oligocene samples from well L13, instead, display a bimodal age-spectrum including a second peak at 400-460 Ma. Shao et al. (2016) suggested local uplifts in the western Pearl River Mouth Basin as a possible source for these zircon grains, which appear unabraded. In addition to the Cretaceous-Jurassic and lower Paleozoic peaks, a significant cluster at ~1000 Ma appears in the upper Oligocene sample from well L21, which yielded a few ages around 1900 and 2500 Ma. The age distributions of the three samples from well X28 also show a progressive increase in Precambrian ages from the lower Oligocene to the lower Miocene, where a broad cluster at 800-1000 Ma and a minor one at ~2500 Ma appear. The middle Miocene sample from well H9 displays a polymodal spectrum including, besides the main peak at ~140 Ma, several age clusters at ~220, ~420, ~800, ~1900, and ~2600 Ma. Such a stratigraphic trend, observed consistently across the Pearl River Mouth Basin, may reflect the progressive westward expansion of the Pearl River, including only the Bei and Dong branches draining eastern Cathaysia in the early Oligocene, and then incorporating by headward erosion first the Hongshui and Yu rivers in the late Oligocene, and next the Liu and Gui rivers in the early Miocene (Pang et al., 2009; Xie et al., 2013; Shao et al., 2016).

4. METHODS

4.1. Sampling

Eight very fine- to very coarse-grained sand samples (Fig. 1) were collected on banks and active bars of major Pearl River branches (samples S5497 = Hongshui; S5498 = You; S5502 = Long; S5504 = Qian; S5507 = He; S5509 = Bei; S5513 = Dong; S5512 = Pearl River mouth). Another five samples were collected from

outside the Pearl River catchment, one modern sand from the Qinzhou Bay (QZW) and four borehole samples from the northern Beibuwan Basin (W10, W11 and W12) and southwestern Pearl River Mouth Basin (W9) (Fig. 2). Stratigraphic ages of borehole samples are based on palaeontological data and 3D seismic (Huang et al., 2013; Liu et al., 2016) (Fig. 3). Further information on sample locations is given in Appendix Table A1 and Supplementary file *Pearl Z. Kmz*.

4.2. Detrital zircon geochronology

U-Pb dating was conducted using an Agilent 7700e ICP-MS instrument coupled to a GeolasPro laser-ablation system at Wuhan Sample Solution Analytical Technology Co., Ltd., Wuhan, China, according to the procedure described in Liu et al. (2008), Hu et al. (2015), and Zong et al. (2017). Cathodo-luminescence (CL) images were used to identify zoning of zircon grains and select the spot for U-Pb and trace-element analysis. The laser spots was systematically placed on both cores and rims of zoned zircon grains. The spot size and frequency of the laser were set to 32 µm and 80 Hz, respectively. Further information on instrumental details and data reduction are provided in Zong et al. (2017). Software ICPMSDataCal (Liu et al., 2008, 2010) was used to calculate U-Pb ages after common Pb correction (Andersen, 2002). We used $^{206}Pb/^{238}U$ and $^{207}Pb/^{206}Pb$ ages for zircons younger and older than 1000 Ma, respectively (Compston et al., 1992). Grains with > 10% age discordance were discarded. Data are visualized as kernel density estimates (KDE) using the Java-based *DensityPlotter* program (Vermeesch, 2012). The selection of adaptive bandwidth of the kernel density estimation is 40 Ma. The complete dataset is provided in Appendix A.

4.3. Seismic reflection data

In order to constrain sediment provenance in the Beibuwan Basin during the Eocene to early Oligocene, we studied an area of ~2000 km^2 entirely covered by three-dimensional seismic-reflection data collected by the China National Offshore Oil Corporation (CNOOC), Zhanjiang Branch. The seismic cube has a bin size of 12.5 × 12.5 m with 2 ms of sample rates. The peak frequency is ~30 Hz, which allows a vertical resolution of ca. 20 m.

5. GEOCHRONOLOGICAL DATA

5.1. Detrital zircon ages in Pearl River sands

5.1.1. Hongshui River

The Hongshui River is formed by the confluence of its Beipan and Nanpan branches (Fig. 1). Literature data indicate multimodal spectra of detrital-zircon ages in modern Beipan (sample R1) (Fig. 6A), Nanpan (sample R2) (Fig. 6B) and upper Hongshui sands (samples 005 (Fig. 6C) and R3 (Fig. 6D)), with a main Permian peak and subordinate early Paleozoic, Neoproterozoic, Mesoproterozoic, Paleoproterozoic, and Neoarchean clusters. Our lower Hongshui River sample S5497 is characterized by prominent peaks at ~265 and ~800 Ma, a subordinate peak at ~90 Ma not appearing in other samples, and by subordinate age clusters at ~430 and ~1830 Ma (Fig. 6E).

5.1.2. Liu River

The Liu River is formed by the confluence of its Long and Rong branches (Fig. 1). All samples display a major peak between 795 and 830 Ma, which is dominant in Liu River sample R6 (Fig. 6I) and in Long River sample 102 (Fig. 6G), where it is associated with a few ages ranging from 920 to 2450 Ma. Rong River sample 105 (Fig. 6H) displays additional clusters at ~530 Ma, ~980, ~2000 and ~2540 Ma. The age spectrum of our Long River sample S5502(Fig. 6F), collected shortly upstream of sample 102, is instead multimodal, with clusters at ~585, ~950, ~1130, ~1770, and ~2435 Ma.

5.1.3. Yu River

The Yu River is formed by the confluence of its You and Zuo branches (Fig. 1). The three samples R4, S5498 and 906 from the You branch all show two peaks at ~275 Ma and ~435 Ma and minor clusters around 1000, 1900 and 2550 Ma (Fig. 6K, M). The two samples R5 and 903 from the Zuo branch are similar, but with a more pronounced Permian peak relative to the early Paleozoic peak and more prominent cluster at ~1900 Ma (Fig. 6O, P). The age spectrum of the Yu River sample 304 downstream is instead more markedly

multimodal, including a major broad cluster around 1000 Ma (Fig. 6Q).

5.1.4. Gui, He, Bei, and Dong tributaries

The two Gui River samples R8 and 501 display multimodal age spectra with a major peak at 1000-1100 Ma, and clusters at 400-700, 1700-1800, and 2500-2550 Ma (Fig. 6b, c). Sample 501 shows an additional young cluster at ~220 Ma. In contrast, all samples from the He, Bei, and Dong Rivers draining the Cathaysian block to the east (Fig. 2) are characterized by a dominant, much younger peak at ~150 Ma. The age distribution in our He River sample S5507 is multimodal, with subordinate peaks at ~420, and ~930 Ma, and minor clusters at ~1800 and ~2500 Ma (Fig. 6d). Among the four Bei River samples, a range of Precambrian ages characterize upstream sample S20 (Fig. 6e) but rapidly decrease in frequency in sample S21 (Fig. 6f) downstream, and samples R10 (Fig. 6g) and S5509 (Fig. 6h) farther downstream are dominated by Cretaceous-Jurassic ages with a minor cluster around 450 Ma. The three Dong River samples R12, S5513 and P1 include a notable peak at ~435 Ma which decreases progressively downstream, and a minor cluster around 1000 Ma that increases slightly downstream (Fig. 6i, j, k).

5.1.5. Trunk river

The trunk river takes the name of Qian after the confluence between the main Hongshui River and the Liu River, the name of Xun downstream of the confluence with the Yu River, and the name of Xi (Lower Xi) downstream of the confluence with the Gui and He rivers (Fig. 1). The age spectrum of the Qian River sample (Fig. 6J) is multimodal, with a main peak around 800 Ma (characteristic of Liu sand (Fig. 6I) but present also in our downstream Hongshui sample (Fig. 6E)), and additional clusters around 260 Ma (characteristic of Hongshui sand (Fig. 6C, D, E)), 535 Ma (present in the Rong (Fig. 6H) and in our Long sand (Fig. 6F) samples), 1810 Ma, and 2435 Ma (present in both Hongshui (Fig. 6C, D, E) and Liu (Fig. 6I) sands). In the Xun River sample R7 (Fig. 6a) downstream, the ~260 and ~450 Ma age peaks characteristic of the Yu River (Fig. 6Q) and its branches are markedly enhanced at the expense of Precambrian clusters.

Age spectra of Xi River samples P7 (Fig. 6m) and R9 (Fig. 6n) are multimodal, with a newly appeared Cretaceous-Jurassic cluster (characteristic of the He River), a somewhat reduced peak at 200-300 Ma, a still

prominent peak at 400-500 Ma, a broad cluster at 800-1100 Ma (reflecting mixed grains from both upstream branches and the Gui River (Fig. 6b, c)), and a few scattered Paleoproterozoic and Neoarchean ages (present in Gui (Fig. 6b, c) and He (Fig. 6d) rivers). Lower Xi River samples SY01 (Fig. 6o) and P4 (Fig. 6p) downstream are more distinctly trimodal, with a major peak at 400-500, a composite cluster between 100 and 300 Ma, and a late Neoproterozoic cluster around 900-1000 Ma. This last cluster is barely expressed in sample R11 (Fig. 6q) collected downstream of the Bei River confluence (Fig. 6). Finally, our sample S5512 displays a simple spectrum dominated by a ~230 Ma peak with a subordinate cluster at ~430 Ma (Fig. 7E).

Spectra from samples S2-5 and C345 collected offshore (Fig. 2) are instead trimodal as in Lower Xi sand, with a major peak around 150 Ma (characteristic of the He, Bei, and Dong Rivers) and subordinate peaks at 400-500 and 800-1000 Ma. An age cluster at 200-300 Ma and scattered Mesoproterozoic to Mesoarchean ages also occur (Fig. 7F, G).

5.2. Detrital zircon ages in offshore basins

Sample QZW from the Qin river mouth displays a simple spectrum virtually identical to our Pearl River mouth sample, with a major peak at ~240 Ma and a few ages at 400-500 and 800-1000 Ma (Fig. 7A).

Our upper Oligocene sample W9 from the Pearl River Mouth Basin displays a prominent age peak at ~425 Ma and a minor cluster at ~230 Ma (Fig. 7H).

All of our three samples from the Beibuwan Basin display a prominent 420-450 Ma age peak. Eocene samples include either a few grains dated as 100-200 Ma (W10) (Fig. 7D) or age clusters at ~250 Ma and ~900 Ma (W11) (Fig. 7C). The lower Oligocene sample (W12) (Fig. 7B) includes minor age clusters at ~265 and ~645 Ma, and a few Paleoproterozoic grains.

6. PROVENANCE IMPLICATIONS

U-Pb ages of detrital zircons in modern Pearl River sands (Fig. 6), compared with geochronological fingerprints of Red River sediments (Fig. 4I) and of basement rocks in North Vietnam, Yangtze Craton, and

Cathaysia Block provide useful provenance information and reflect relative supply of zircon grains within this complex modern drainage network.

6.1. Zircon-age fingerprints of Pearl River sand

The prominent 100-200 Ma peak displayed in Lower Xi River sand and in samples S2-5 and C345 collected offshore of the Pearl River mouth (Fig. 7F, G) highlights a major contribution from the He, Bei, and Dong rivers, which drain the eastern Cathaysia Block where Yanshanian granites are extensively exposed (Xu et al., 2007; Zhao et al., 2015; Liu et al., 2017). In comparison to samples S2-5 and C345 (Fig. 7F, G), the Pearl River mouth sample S5512 collected along the river bank in the delta (Fig. 7E) lacks the 100-200 Ma peak, a discrepancy that may be explained by seasonal variability in sediment supply with greater input from locally exposed Indosinian granites and Silurian granites and Precambrian basement in the near north.

The 230-250 Ma zircon ages yielded by river mouth and offshore samples S5512, S2-5, and C345 (Fig. 7E, F ,G) correspond to the age of Indosinian granites (Fig. 4B) widely represented in SE Tibet and in the westernmost part of the catchment drained by the diverse branches of the Hongshui and Yu rivers. Additional zircon grains dated as 230-250 Ma may be supplied by Indosinian granites found in the Yunkai Massif (Fig. 4G) or scattered in other parts of the catchment (Fig. 2).

The 435-440 Ma aged zircons found in river mouth and offshore samples S5512, S2-5, and C345 are ultimately derived from Silurian granites (Fig. 4D) presently exposed in the Jiangnan orogen, Cathaysia Block, and Yunkai Massif (Fig. 2), and mainly contributed both from the upper catchment and from the He and Dong rivers in the lower catchment (Zhao et al., 2015; Liu et al., 2017) (Figs. 6d, i, j and 7k).

The 800-1000 Ma aged zircons found in Lower Xi River and offshore sediments are most characteristic of the Liu (Fig. 6l) and Gui (Fig, 6b, c) rivers, and also occur in the Hongshui, Yu, and He catchments (Fig. 6). Zircons of these ages may derive from the Chuandian fragment (Fig. 4E), the Jiangnan orogeny (Fig. 4F), the Yunkai Massif (Fig, 4G), or from eastern Cathaysia. Zircon grains yielding Mesoproterozoic to Mesoarchean ages are either derived from old basement rocks or recycled from siliciclastic cover strata.

6.2. Relative zircon contributions

A simple and powerful statistical technique apt to assist the interpretation of large detrital-geochronology datasets is multidimensional Scaling (MDS), which produces a map of points in which samples with similar age spectra cluster closely together and dissimilar samples plot far apart (Vermeesch,2013; Vermeesch and Garzanti, 2015). The goodness of fit of the configuration can be evaluated using the final stress value according to Kruskal (1964; Vermeesch, 2018), which is 0.094 for our dataset, indicating a good to fair fit (Fig. 8).

In the upper Pearl River catchment, both Beipan sample R1 and Nanpan sample R2 closely group in the MDS plot together with Hongshui samples 005, R3 and S5497, Nanpan sample R2 plotting closest to them. The Nanpan branch is thus suggested to contribute more zircon grains than the Beipan River to the Hongshui River downstream. Both You samples R4, S5498 and 906 and Zuo sample R5 group quite far from the Yu samples 903 and 304 downstream (Fig. 8), which is hard to explain. The two Long River samples 102 and S5502 and Rong River sample 105 group with Liu River sample R6, suggesting that both Long or the Rong branches contribute significant and roughly subequal amounts of zircon grains to the Liu River downstream. Also the relative zircon contribution of the Hongshui River (samples 005, R3 and S5497) and Liu River (sample R6) to the Qian segment (sample S5504), and by the Yu River (sample 304) to the Xun segment (sample R7) cannot be precisely assessed.

Dong River samples R12, S5513 and P1, Bei River samples S21, S5509 and R10, Lower Xi sample R11, and Pearl River mouth sample S5512 all group relatively close together. River mouth samples S2-5 and C345 plot close to the He River sample S5507 and to samples from the west Qian and Xun branches (Fig. 8). Sample QZW from the Qin River is closest to the Zuo River sample R5 and relatively close to the Pearl Rriver mouth sample S5512, which suggests supply from Indosinian granites exposed in the Shiwandashan Belt (SWSB) to the Zuo and Qin Rivers and instead from Indosinian granites exposed near the Pearl River mouth to sample S5512. Age-spectra in Lower Xi, river mouth and offshore samples are variable, but overall they indicate significant contribution from the Qian and Xun segments upstream (characteristic peaks at ~260, ~450, and ~ 800 Ma) as well as from the Gui (~1000 Ma peak), He (~150 Ma, ~420, and ~930 Ma), and Dong (~435 Ma peak) tributaries downstream (Fig. 6).

6.3. Zircon-age fingerprints of offshore basin sediments

A comparison of zircon-age spectra in modern sediments *versus* Cretaceous to Cenozoic strata in offshore boreholes provides fundamental provenance information useful to reconstruct the evolution of the Pearl River through time (Figs. 5, 6, and 7).

6.3.1. Pearl River Mouth Basin

The Upper Oligocene sample W9, located in the western part of the basin far from the Pearl River mouth and close to Hainan Island, displays a prominent Silurian age peak and only a minor Indosinian cluster (Fig. 7H). Its zircon age distribution, therefore, is notably different from that in both modern Pearl River sand and coeval Upper Oligocene samples (X28, L18, L21, and L13) (Fig. 5E, G, I, M) collected in the central and eastern parts of the basin. The bedrocks of Hainan Island are dominated by Mesozoic Yanshanian and Indosinian granites (Fig. 2; Cao et al., 2015; Wang et al., 2015; Xu et al., 2014), which precludes major sediment contribution from Hainan Island. The Yunkai Massif, instead, is characterized by extensive exposure of Silurian granites (Fig. 4), and may thus represent the source area for sample W9 *via* a southward-flowing stream comparable to the modern Jian River (Fig. 2). This is corroborated by the finding of zircon grains with early Paleozoic age in sediments deposited close to the Jian River mouth (Zhong et al., 2017).

6.3.2. Beibuwan Basin

A possible sediment source for the Beibuwan Basin is represented by the Red River, which flows along the Red River strike-slip fault zone active since ~34 Ma (Gilley et al., 2003; Clift et al., 2006). During the Oligocene, however, the Red River provided sediments chiefly to the Yinggehai-Song Hong Basin (YSB in Fig. 2; Yan et al., 2011; Clift et al., 2006; C. Wang et al., 2014, 2018; Jiang et al., 2015; Lei et al., 2019), where lower Oligocene samples are characterized by a major Indosinian peak (Shao et al., 2016; Lei et al., 2019). The main peak in our Eocene to lower Oligocene samples (W10, W11, W12) from the Beibuwan Basin is

much older (~450 Ma; Fig. 7B, C, D), which precludes major sediment contribution from the Red River at those times.

Hoang et al. (2009) suggested that the Beibuwan Basin received sediments from the paleo-Pearl River originating from the Tibetan Plateau margin in the Cenozoic. The Silurian age mode is in fact present in samples from the Xi, Dong, Xun, and You rivers of the modern Pearl River catchment (Figs. 6 and 7). According to Li et al. (2017), however, the Shiwandashan belt (SWSB in Fig. 2) had already formed in the Late Permian in response to subduction of the paleo-Pacific and collision between Indochina and South China. As a consequence, paleo-Pearl River sediments are unlikely to have crossed the Shiwandashan belt to enter the Beibuwan Basin in the Cenozoic.

The prominent Silurian zircon-age peak characterizing our three Beibuwan Basin samples indicates the Yunkai Massif as the most likely source. The northwestward paleocurrent indicators shown in Fig. 2 indicate the Yunkai Massif and Shiwandashan belt as the sediment source for the Upper Permian to Lower Triassic siliciclastic succession deposited in the Shiwandashan belt (Hu et al., 2015). In a similar way, sediments from the Yunkai Massif may have been transported to the northern Beibuwan Basin *via* a westward- or southwestward-flowing stream similar to the modern Qin River flowing along the Qin Fang shear zone (Fig. 2).

There are however some difficulties with this hypothesized sediment route. The zircon-age spectrum in modern sand sample QZW (Fig. 7A) from the Qin River mouth is dominated by an Indosinian peak and notably different from that characterizing our three Beibuwan Basin samples (Fig. 7B, C, D), pointing to a local source in Indosinian granites of the Shiwandashan belt. Moreover, a buried carbonate ridge marks the northern margin of the Beibuwan Basin (Jiang et al., 2018) and seismic-reflection images document a set of large eastward-prograding deltas in the Upper Eocene Liushagang Formation (Fig. 9). If the Yunkai Massif was indeed the main source of our Eocene and Oligocene samples, then the sediment-transport path may have been first northwestward and then should have turned southwestward to enter the sea, and finally eastward around the buried carbonate ridge that marks the northern margin of the Beibuwan Basin (Jiang et al., 2018), possibly following the ENE/WSW-directed No.1 Fault (Fig, 8). At any rate, based on the

considerations made above, the paleo-Pearl River is ruled out as a sediment source for the Eocene-Oligocene Beibuwan Basin.

7. HISTORY OF THE PEARL RIVER CATCHMENT

U-Pb ages of detrital zircons in modern Pearl River sands (Fig. 6), compared with geochronological fingerprints of Lower Cretaceous to middle Miocene strata cored in the Pearl River Mouth Basin (Fig. 5) provide provenance information useful to reconstruct the evolution of landscape in the vast region comprised between SE Tibet and the South China Sea through time. Six stages are identified (Fig. 10).

In agreement with Clift et al. (2002), we consider that the Pearl River drainage progressively expanded westward inland from the South China margin in response to Cenozoic uplift of the Tibetan Plateau, evolving separately from the Red River and Yangtze River. This because of the following reasons: 1) the Pb isotope fingerprint of detrital K-feldpars in Eocene sediments offshore of the Red River mouth is similar to that of bedrocks in the Yangtze Craton and different from any other known potential source in eastern Asia (Clift et al., 2004, 2006). Therefore, the paleo-Pearl River is unlikely to have been part of the paleo-Red River catchment in the Eocene; 2) paleocurrent data from fluvial conglomerates exposed between the Red River and the Nanpan River indicate that the Red River and Pearl River drainages have remained separated since the Eocene (Wissink et al., 2016; Cao et al., 2018); 3) ^{40} Ar/^{39} Ar dating of basalts and U-Pb zircon dating of gravels show that the Yangtze River initiated before 23 Ma by headwater capture of upper reaches of the Red River (Zheng et al., 2013).

7.1. Early Cretaceous

During the Early Cretaceous, the Andean-type arc was fed by subduction of the paleo-Pacific Ocean beneath the South China margin (Lapierre et al., 1997; Li et al., 2012; Yan et al., 2014; Sun, 2016; C. Xu et al., 2016, 2017; Ye et al., 2018). The 185 Ma peak dominating the unimodal detrital-zircon spectrum of Lower Cretaceous sample L35 points to a source in earliest Yangshanian magmatic-arc rocks exposed along the South China margin (Zhou and Li, 2000; Li et al., 2012; Shao et al., 2017a) (Fig. 5). Lack of older age

populations in sample L35 – apart from a few 1800-2000 Ma zircons, possibly recycled and ultimately derived from old basement rocks of the Cathaysia Block (Zhou and Li, 2000; Li et al., 2012; Shao et al., 2017a) – precludes provenance from the South China hinterland through long-distance transport. Moreover, as a consequence of paleo-Pacific subduction and related magmatism, topography was presumably much higher in eastern South China than in the west at that time. Zircon grains were thus supplied to the Pearl River Mouth Basin by a short and steep coastal river sourced in the Andean-type arc formed along the southeastern margin of Cathaysia. This coastal river, initiated in the east and thus considered as a paleo-Dong, may have represented the first original segment of the Pearl River (Fig. 10a).

7.2. Late Cretaceous

The geodynamic scenario changed during the early late Cretaceous, after the Pacific-Izanagi ridge was subducted beneath the South China margin and the Izanagi plate became part of the Pacific plate (Fig. 10b; Engebretson, 1985; Maruyama et al., 1997; Ye et al., 2018). This change in plate configuration led to slab retreat, onset of strong back-arc extension, and transformation of the previous Andean-type margin into a new Western Pacific-type active margin (Zhou and Li, 2000; Shu et al., 2009; Wang and Shu, 2012; Sun, 2016). Rifting in the proto-South China Sea induced formation of sedimentary basins along its northern margin and initial southward migration of the micro-continental blocks found today along its the southern margin (Morley, 2012; Wang and Shu, 2012; Bai et al., 2015; Ye et al., 2018). In coastal SE China, two main groups of magmatic rocks can be distinguished, namely, lower Yanshanian (180-140 Ma; J_2-J_3) and upper Yanshanian (140-97 Ma; K_1). The zircon-age peak dominating the unimodal spectrum of sample L35* (Fig. 5N) is younger than in the older sample L35 (Fig. 5O), and matches the age of upper Yanshanian igneous rocks emplaced in coastal South China (Chen et al., 2000, 2008; Zhou and Li, 2000; Shao et al., 2017a; Ye et al., 2018).

As a result of extension and crustal thinning, topographic relief continued to increase throughout the Cretaceous in the eastern Cathaysia Block (Lapierre et al., 1997; Zhou et al., 2006; Ye et al., 2018), where existence of a coastal mountain range is supported by stratigraphic, paleoaltimetric, and paleoclimate studies (Zhou and Li, 2000; J. Li et al., 2014; Zhang et al., 2016). Based on the available evidence, the most

likely scenario is that the Pearl River expanded its catchment starting from the South China margin and subsequently progressing westward by headward erosion. We infer that the paleo-Dong River might have incorporate a paleo-Bei River at that time (Fig. 10b).

7.3. Paleocene-Eocene

Continental rifting that preceded opening of the South China Sea initiated in the Paleocene (e.g., Cullen et al., 2010; Savva et al., 2014; Morley, 2016; Ye et al., 2018). At the same time, the proto-South China Sea began to subduct beneath the northern edge of the Sabah-Cagayan and Borneo arc (Hall, 2012; Hall and Breitfeld, 2017), with possible causal relationship between subduction in the south and rifting in the north (Taylor and Hayes, 1983; Morley, 2002; Hall and Breitfeld, 2017). Elevation decreased in eastern South China but remained higher than in the west (Fig. 10 l ; Wang et al., 2004). Only modest headward expansion of the proto-Pearl River catchment took place at this stage. Very young zircon ages (110-115 Ma), with only a few 200-300 Ma grains, are dominant in Eocene samples from boreholes U1435 (Fig. 5A) and L21 (Fig. 5J), which may reveal provenance from exhumed basement rocks of the Pearl River Mouth Basin (Shi et al., 2011; Shao et al., 2017b) rather than from the paleo-Bei and paleo-Dong rivers. The Beibuwan Basin, instead, was most likely fed from the northeastern Yunkai Massif, as discussed above (Fig. 10c).

7.4. Early Oligocene

After break-up and initiation of sea-floor spreading (Morley, 2016), elevation of the eastern Cathaysia block progressively decreased. At the same time, rapid uplift began in southeastern Tibet (Dupont-Nivet et al., 2008; G. Wang et al., 2011). Southward-prograding deltaic clinoforms documented by seismic-reflection data from the northern Pearl River Mouth Basin indicate onset of major fluvial supply from the paleo-Pearl River (Pang et al., 2009; Cao et al., 2018). Samples X28 and L13 farther south yielded mostly Yanshanian zircons, subordinate Indosinian and Silurian zircons, and few Proterozoic grains (Fig. 5E, M) indicating provenance from eastern Cathaysia only (paleo-Bei + paleo-Dong), without contribution from the central and western parts of the modern catchment (Fig. 10d). Rather, additional contributions from local uplifts in

the western part of the Pearl River Mouth Basin have been suggested for sample L13 (Pang et al., 2009; Xie et al., 2013; Shao et al., 2016). A limited extent of the paleo-Xi River was also indicated by Monte Carlo-based sediment-unmixing analysis (Cao et al., 2018). Occurrence of well-rounded zircon grains, suggested to indicate a relatively long distance transport (Shao et al., 2016), may reflect eolian abrasion or recycling as well (Dott, 2003).

The unimodal spectrum of sample L18, dominated by typically euhedral zircons with ages varying from 100 to 200 Ma (Fig. 5G), points to a distinct local source, possibly represented by the Dongsha Uplift (C. Li et al., 2014; Shao et al., 2016). Detritus from the same source may have travelled farther south to reach the locality of sample L21*, which displays a similar age distribution (Fig. 5I; Shao et al., 2016; Cao et al., 2018). Detritus from the northeastern Yunkai Massif continued to feed the Beibuwan Basin (Fig. 10d).

7.5. Late Oligocene

Transition to the post-rift stage in the northern South China Sea margin (Forsyth and Uyeda, 1975) and accelerated surface uplift of the eastern Tibetan Plateau (G. Wang et al., 2011) produced a major change in the topography of South China, now more elevated in the west than in the east (Fig. 10III; Wang et al., 2004). A major transgression in the northern South China Sea was documented by a facies change from lacustrine and restricted-marine to open-neritic environments (Zhao et al., 2009; Shao et al., 2016). Zircon-age spectra remain fundamentally unchanged at sites X28, L18, and L13 (Fig. 5D, F, K), whereas sample L21** shows newly-appeared peaks at 420-430 Ma and 960-995 Ma comparable to the spectra characterizing modern Pearl River sediments (Figs. 6 and 7H). This indicates that the paleo-Lower Xi River had expanded farther, and possibly much farther to the west, incorporating the paleo-He and paleo-Gui River, and probably part of the upper branches as well (Fig. 10e). A few more Proterozoic zircons in sample X28* may have been derived from an additional source in inland South China (Cao et al., 2018), as suggested by the negative Nd isotopic excursion recorded in late Oligocene sediments cored at ODP Site 1148 in the Pearl River Mouth Basin (Fig. 2; Clift et al., 2002; Li et al., 2003b; Shao et al., 2008b).

7.6. Early to middle Miocene

Active sea-floor spreading in the South China Sea resulted in the southward migration of the Reed Bank, Dangerous Grounds and Palawan-Mindoro blocks, while the proto-South China Sea was gradually consumed by subduction (Hall, 2002, 2012; Hall and Breitfeld, 2017) (Fig. 10e). Continuing rapid uplift of the Tibetan Plateau enhanced elevation and relief in western China. The sharp increase in Silurian and Neoproterozoic zircons at site X28 indicates additional supply from the Jiangnan orogen and/or Chuandian fragment (Fig. 5C), suggesting that the paleo-Pearl River had reached a configuration similar to the present day in the early Miocene (Fig. 10f). This is corroborated by the similarity of zircon-age spectra in samples X28** (Fig. 5C) and H9 (Fig. 5B) with samples S2-5 (Fig. 7F) and C345 (Fig. 7G) from the modern Pearl River mouth (Figs. 5 and 7) and by Nd isotope data (Clift et al., 2002; Shao et al., 2008b).

8. CONCLUSION

The comparison of original and literature data on the age of detrital zircons in modern sands of the Pearl River catchment and in ancient strata cored in sedimentary basins offshore allowed us to reconstruct the geological and geomorphological evolution of southern China from the Early Cretaceous to the present day. Six main stages are identified:

(1) Early Cretaceous: elevated topography characterized the eastern South China margin, where an elevated Andean-type magmatic belt was formed in response to subduction of the paleo-Pacific plate. Detrital zircons in the Pearl Mouth River Basin were largely sourced by arc-related granitoids *via* a short coastal stream that may considered as the paleo-Dong.

(2) Late Cretaceous: onset of back-arc extension and rifting of the proto-South China Sea led to formation of rift basins in the northern South China Sea and enhanced topography and relief in South China. The paleo-Dong might have incorporated a paleo-Bei River at that time.

(3) Paleocene to Eocene: after initiation of rifting in the South China Sea, topography became more subdued in South China, but still higher in the east than in the west. Local uplifts supplied sediment to the Pearl River Mouth Basin, whereas the proto-Pearl River remained short and chiefly confined to the paleo-Dong and paleo-Bei catchments in the east. The northern Beibuwan Basin received sediments

locally from the Yunkai massif rather than from the paleo-Pearl River.

(4) Early Oligocene: rapid uplift of SE Tibet in the west and progressively reduced elevation in the east after onset of sea-floor spreading in the South China Sea fostered increased sediment supply and progradation of the paleo-Pearl River delta, as documented by seismic-reflection data. Nonetheless, zircon-age spectra indicate that the paleo-Pearl River catchment remained chiefly confined to the paleo-Bei and paleo-Dong rivers only, without contributions from the central and western parts of the modern catchment. Detritus from the northeastern Yunkai Massif continued to supply the Beibuwan Basin.

(5) Late Oligocene: accelerated uplift of SE Tibet and transition to post-rift sagging in the north South China Sea margin led to a reversal in the topography of South China, now more elevated in the west as it is today. The paleo-Pearl River rapidly expanded westward, incorporating part of the modern upper branches.

(6) Early to middle Miocene: topographic relief in South China and the paleo-Pearl River catchment eventually reached a configuration similar to the present, as documented by similar zircon-age distributions in samples from Miocene strata of the Pearl River Mouth Basin and from the modern river mouth.

ACKNOWLEDGEMENTS

This paper was supported by the Major National Science and Technology Programs in the “Thirteenth Five-Year” Plan period (No.2016ZX05024-006-002), and the Zhanjiang Branch of China National Offshore Oil Corporation. We greatly thank Yunfei Shangguan and Xiangrong Yang for sampling, and Xiong Pang, Chaoqun Yang, Renzhi Zhu and Guanzhong Shi for beneficial discussions, and Alberto Resentini for help in the statistical analysis of the geochronological dataset. Pieter Vermeesch and J.E. Saylor kindly offered careful constructive comments during the revision process and Editor Luca Caracciolo handled the manuscript very efficiently.

SUPPLEMENTARY MATERIAL

Supplementary detrital-zircon geochronology data associated with this article is to be found as Appendix A in the online version at http://dx.doi._____. Information on sampling sites is provided in Appendix Table A1 and in the Google-Earth map Pearl Z.kmz.

FIGURE CAPTIONS

Fig. 1. Topographic map of the Pearl River catchment, showing tributaries and location of sampling sites.

Fig. 2. Geological map of South China and location of offshore samples. Two black arrows in the upper Nanpan River valley and three black arrows west of the Qin River indicate northeastward and northwestward paleocurrent directions in Eocene (Wissink et al., 2016) and Upper Permian to Lower Triassic strata (Hu et al., 2015), respectively. The blue dashed line and the thick black dashed line indicate the boundary between the Yangtze craton and Cathaysia block and the limit of the Pearl River catchment, respectively. BBW: Beibuwan Basin; DS: Dongsha Island; HN: Hainan Island; PRD: Pearl River Delta; PRMB: Pearl River Mouth Basin; SWSB: Shiwandashan Belt; YSB: Yinggehai-Song Hong Basin (after Chinese Geology Survey, 2010; Y. Xu et al., 2016; Cao et al., 2018).

Fig. 3. Stratigraphic framework and age of borehole samples used in this study from the northern South China Sea (after Huang et al., 2013; Liu et al., 2016; Shao et al., 2016, 2017; Cao et al., 2018).

Fig. 4. Compilation of U-Pb ages of detrital zircons from bedrock units in different tectonic domains drained by the Pearl River. The main source of data is indicated in each label; other sources include: 1) Shellnutt et al. (2012) and Wang et al. (2012) for Indosinian granites; Song et al. (2015) for Silurian granites; Zhou et al. (2002), Li et al. (2002), and Cui et al. (2015) for the Chuandian Fragment; Wang et al. (2006), Li (1999), and X. Wang et al. (2014) for the Jiangnan Orogen; Hu et al. (2015), Yu et al. (2010), Peng et al. (2006), Qin et al. (2006), A. Zhang et al. (2012), Chen et al. (2012), Zhao et al. (2010), Chen et al. (2011) for the Yunkai Massif; Song et al. (2015), Hu et al. (2015), and Tran et al. (2008) for North Vietnam; Clift et al. (2006b) for the Red River. Age vs. frequencies plotted as kernel density estimates using the provenance package of Vermeesch et al. (2016); n = number of concordant ages.

Fig. 5. Compilation of U-Pb ages of detrital zircons from Lower Cretaceous to middle Miocene strata of offshore basins (data sources indicated in each label). Age vs. frequencies plotted as kernel density estimates (Vermeesch et al., 2016); n = number of concordant ages.

Fig. 6. U-Pb age spectra of detrital zircons in modern sands of Pearl River tributaries (data sources indicated in each label; own data labelled in blue). Age vs. frequencies plotted as kernel density estimates (Vermeesch et al., 2016); n = number of concordant ages.

Fig. 7. U-Pb age spectra of detrital zircons from modern sand of the Pearl River mouth and modern and Cenozoic sediments of offshore basins (data sources indicated in each label; own data labelled in blue). Age vs. frequencies plotted as kernel density estimates (Vermeesch et al., 2016); n = number of concordant ages, PR: Pearl River.

Fig. 8. (a) Nonmetric multidimensional scaling (MDS) map for the detrital zircon U-Pb ages of modern sands of the Pearl River drainage basin and the river mouth using the Kolmogorov-Smirnov (K-S) test statistic. As the distance between two samples is greater, the dissimilarity between the two age distributions is larger. (b) Shepard plots of the nonmetric MDS. The nonmetric MDS solve for the configuration that determines both the distance (blue circles) and the fit to the disparity transformation (red circles and lines) between all possible sample pairs. The stress values of MDS statistics interpret a good to fair goodness of fit. The data sources is the same as in Figures 1 and 2. The colours of different river tracts is in accordance with previous Figures 6 and 7.

Fig. 9. Seismic-reflection profile along the northern edge of the Beibuwan Basin (location indicated in inset). The offlap pattern of seismic reflectors indicates eastward sediment progradation in the Upper Eocene Liushagang Formation.

Fig. 10. Envisaged paleogeographic evolution of the Pearl River drainage basin from Early Cretaceous to middle Miocene times (panels **a** to **f**; after Holloway, 1981; Taylor and Hayes, 1983; Morley, 2002; Ye et al., 2018). Profiles **I** to **III** above outline the radical topographic change inferred to have occurred

in South China between the Paleogene and the Neogene (after Wang, 2004). Yellow and green colours represent high and low topography, respectively. MI-Mindoro block; PB-Palawan block; RB-Reed Bank; MB-Macclesfield Bank; PI-Paracel Islands; DG-Dangerous Ground; LB-Luconia block; SCA-Sabah-Cagayan arc.

REFERENCES

Andersen, T., 2002. Correction of common lead in U–Pb analyses that do not report 204Pb. Chemical geology 192(1-2), 59-79.

Bai, Y.L., Wu, S.G., Liu, Z., Müller, R.D., Williams, S.E., Zahirovic, S., Dong, D.D., 2015. Full-fit reconstruction of the South China Sea conjugate margins. Tectonophysics 661, 121–135.

Botsyun, S., Sepulchre, P., Donnadieu, Y., Risi, C., Licht, A., Rugenstein, J.K.C., 2019. Revised paleoaltimetry data show low Tibetan Plateau elevation during the Eocene. Science 363(6430), eaaq1436.

Borges, J.B., Huh, Y., Moon, S., Noh, H., 2008. Provenance and weathering control on river bed sediments of the eastern Tibetan plateau and the Russian Far East. Chem. Geol. 254, 52–72.

Cao, L., Jiang, T., Wang, Z., Zhang, Y., Sun, H., 2015. Provenance of Upper Miocene sediments in the Yinggehai and Qiongdongnan basins, northwestern South China Sea: Evidence from REE, heavy minerals and zircon U–Pb ages. Mar. Geol. 361, 136–146.

Cao, L., Shao, L., Qiao, P., Zhao, Z., van Hinsbergen, D.J., 2018. Early Miocene birth of modern Pearl River recorded low-relief, high-elevation surface formation of SE Tibetan Plateau. Earth and Planetary Science Letters 496, 120-131.

Castelltort, S., Goren, L., Willett, S.D., Champagnac, J.D., Herman, F., Braun, J., 2012. River drainage patterns in the New Zealand Alps primarily controlled by plate tectonic strain. Nature Geosciences 5, 744–748.

Cawood, P. A., Nemchin, A. A., Freeman, M., Sircombe, K., 2003. Linking source and sedimentary basin: detrital zircon record of sediment flux along a modern river system and implications for provenance studies. Earth and Planetary Science Letters 210(1-2), 259-268.

Charvet, J., Lapierre, H., Yu, Y.W., 1994. Geodynamic significance of the Mesozoic volcanism of southeastern China. J. Asian Earth Sci. 9 (4), 387–396.

Chen, C.H., Lee, C.Y., Lu, H.Y., Hsieh, P.S., 2008. Generation of late cretaceous silicic rocks in SE China: Age, major element and numerical simulation constraints. J. Asian Earth Sci. 31 (4–6), 479–498.

Chen, C.H., Lin, W., Lu, H.Y., Lee, C.Y., Tien, J.L., Lai, Y.H., 2000. Cretaceous fractionated I-type granitoids and metaluminous A-type granites in SE China: the late Yanshanian post-orogenic magmatism. Transactions of the Royal Society of Edinburgh Earth Sciences 91 (1–2), 195–205.

Chen, C.H., Hsieh, P.S., Lee, C.Y., Zhou, H.W., 2011. Two episodes of the Indosinian thermal event on the South China Block: constraints from LA–ICPMS U–Pb zircon and electron microprobe monazite ages of the Darongshan S-type granitic suite. Gondwana Res. 19, 1008-1023.

Chen, C.H., Liu, Y.H., Lee, C.Y., Xiang, H., Zhou, H.W., 2012. Geochronology of granulite, charnockite and gneiss in the poly-metamorphosed Gaozhou Complex (Yunkai Massif), South China: emphasis on the in-situ EMP monazite dating. Lithos 106, 83-92.

Chen, S.Z., Pei, C.M., 1993. Geology and geochemistry of source rocks of the eastern Pearl River mouth basin, South China Sea. J. Asian Earth Sci. 8, 393–406.

Chinese Geology Survey, 2010. China Geology Map. Chinese Geology Survey, Beijing, China.

Chu, Y., Lin, W., Faure, M., Wang, Q., Ji, W., 2012. Phanerozoic tectonothermal events of the Xuefengshan Belt, central South China: Implications from UPb age and LuHf determinations of granites. Lithos 150, 243-255.

Clark, M.K., Schoenbohm, L.M., Royden, L.H., Whipple, K.X., Burchfiel, B.C., Zhang, X., Tang, W., Wang, E., Chen, L., 2004. Surface uplift, tectonics, and erosion of eastern Tibet from large-scale drainage patterns. Tectonics 23, TC1006.

Clift, P.D., 2015. Assessing effective provenancemethods for fluvial sediment in the South China Sea. Geol. Soc. Lond. Spec. Publ. 429.

Clift, P.D., 2016. Assessing effective provenance methods for fluvial sediment in the South China Sea. In: Clift, P.D., Harff, J., Wu, J., Qui, Y. (Eds.), River-Dominated Shelf Sediments of East Asian Seas. 429 Geological Society of London, London.

Clift, P., Lin, J., 2001. Preferential mantle lithospheric extension under the South China margin. Marine and Petroleum Geology 18(8), 929-945.

Clift, P.D., Lee, J.I., Clark, M.K., Blusztajn, J., 2002. Erosional response of South China to arc rifting and monsoonal strengthening; a record from the South China Sea. Marine Geology 184, 207–226.

Clift, P.D., Layne, G.D., Blusztajn, J., 2004. The erosional record of Tibetan uplift in the East Asian marginal seas. Continent–Ocean Interactions in the East Asian Marginal Seas, American Geophysical Union, 255-282.

Clift, P.D., Blusztajn, J., Nguyen, A.D., 2006a. Large-scale drainage capture and surface uplift in eastern Tibet – SW China before 24 Ma inferred from sediments of the Hanoi Basin, Vietnam. Geophysical Research Letters 33(19).

Clift, P.D., Carter, A., Campbell, I.H., Pringle, M.S., Van Lap, N., Allen, C.M., Hodges, K.V., Tan, M.T., 2006b. Thermochronology of mineral grains in the Red and Mekong Rivers, Vietnam: Provenance and exhumation implications for Southeast Asia. Geochemistry, Geophysics, Geosystems 7(10).

Clift, P. D., Long, H. V., Hinton, R., Ellam, R. M., Hannigan, R., Tan, M. T., Blusztajn, J., Duc, N. A., 2008. Evolving east Asian river systems reconstructed by trace element and Pb and Nd isotope variations in modern and ancient Red River-Song Hong sediments. Geochemistry, Geophysics, Geosystems 9(4).

Compston, W., Williams, I.S., Kirschvink, J.L., Zichao, Z., Guogan, M.A., 1992. Zircon U-Pb ages for the Early Cambrian time-scale. Journal of the Geological Society 149(2), 171-184.

Cui, X., Jiang, X., Wang, J., Wang, X., Zhuo, J., Deng, Q., Liao, S., Wu H., Jiang, Z., Wei, Y., 2015. Mid-Neoproterozoic diabase dykes from Xide in the western Yangtze Block, South China: New evidence for continental rifting related to the breakup of Rodinia supercontinent. Precambrian Research 268, 339-356.

Cullen, A., Reemst, P., Henstra, G., Gozzard, S., Ray, A., 2010. Rifting of the South China Sea: new perspectives. Petroleum Geoscience 16, 273–282.

DeCelles, P.G., Kapp, P., Gehrels, G.E., Ding, L., 2014. Paleocene–Eocene foreland basin evolution in the Himalaya of southern Tibet and Nepal: Implications for the age of initial India-Asia collision. Tectonics 33, 824–849.

Dott, R.H., 2003. The Importance of Eolian Abrasion in Supermature Quartz Sandstones and the Paradox of Weathering on Vegetation-Free Landscapes. The Journal of Geology 111, 387–405.

Dupont-Nivet, G., Hoorn, C., Konert, M., 2008. Tibetan uplift prior to the Eocene-Oligocene climate transition: Evidence from pollen analysis of the Xining Basin. Geology 36(12), 987-990.

Engebretson, D.C., 1985. Relative motions between oceanic and continental plates in the Pacific basin. Vol. 206 Geological Society of America.

Forsyth, D., Uyeda, S., 1975. On the relative importance of the driving forces of plate motion. Geophys. J. Int. 43 (1), 163–200.

Gaillardet, J., Dupré, B., Allègre, C.J., 1999. Geochemistry of large river suspended sediments: silicate weathering or recycling tracer? Geochim. Cosmochim. Acta 63, 4037–4051.

Garzanti, E., 2016. From static to dynamic provenance analysis—Sedimentary petrology upgraded. Sedimentary Geology 336, 3-13.

Garzanti E., 2017. The maturity myth in sedimentology and provenance analysis. Journal of Sedimentary Research 87, 353-365.

Garzanti, E., Wang, J.G., Vezzoli, G., Limonta, M., 2016. Tracing provenance and sediment fluxes in the Irrawaddy River basin (Myanmar). Chemical Geology 440, 73-90.

Garzanti, E., Vermeesh, P., Rittner, M., Simmons, M., 2018. The zircon story of the Nile: time-structure maps of source rocks and discontinuous propagation of detrital signals. Basin Research 30, 1098-1117.

Gilley, L.D., Harrison, T.M., Leloup, P.H., Ryerson, F.J., Lovera, O.M., Wang, J.H., 2003. Direct dating of left - lateral deformation along the Red River shear zone, China and Vietnam. Journal of Geophysical Research: Solid Earth, 108(B2).

Hall, R., 2002. Cenozoic geological and plate tectonic evolution of SE Asia and the SW Pacific: computer-based reconstructions, model and animations. J. Asian Earth Sci. 20 (4), 353–431.

Hall, R., 2012. Late Jurassic-Cenozoic reconstructions of the Indonesian region and the Indian Ocean. Tectonophysics 570-571 (11), 1–41.

Hall, R., Breitfeld, T., 2017. Nature and demise of the proto-southChina sea. Bulletin of the Geological Society of Malaysia 63, 61–76.

He, Z.Y., Xu, X.S., 2012. Petrogenesis of the late Yanshanian mantle-derived intrusions in Southeastern China: response to the geodynamics of Paleo-Pacific Plate subduction. Chem. Geol. 328 (11), 208–221.

Hinderer, M., 2012. From gullies to mountain belts: a review of sediment budgets at various scales. Sediment. Geol. 280, 21–59.

Hoke, G.D., Liu, -Z.J., Hren, M.T., Wissink, G.K., Garzione, C.N., 2014. Stable isotopes reveal high southeast Tibetan Plateau margin since the Paleogene. Earth and Planetary Science Letters 394, 270–278.

Holloway, N.H., 1981. The North Palawan block, Philippines: its relation to the Asian mainland and its role in the evolution of the South China Sea. Geological Society of Malaysia Bulletin 14, 19–58.

Hu, D., Clift, P.D., Böning, P., Hannigan, R., Hillier, S., Blusztajn, J., Wang, S., Fuller, D.Q., 2013. Holocene evolution in weathering and erosion patterns in the Pearl River delta. Geochem. Geophys. Geosyst. 14.

Hu, L., Cawood, P. A., Du, Y., Xu, Y., Xu, W., Huang, H., 2015. Detrital records for Upper Permian-Lower Triassic succession in the Shiwandashan Basin, South China and implication for Permo-Triassic (Indosinian) orogeny. Journal of Asian Earth Sciences 98, 152-166.

Hu, X.M., Garzanti, E., Wang J.G., Huang, W., An, W., Webb, A., 2016. The timing of India-Asia collision onset – facts, theories, controversies. Earth-Science Reviews 160, 264-299.

Huang, B., Tian, H., Wilkins, R.W.T., Xiao, X., Li, L., 2013. Geochemical characteristics, palaeoenvironment and formation model of Eocene organic-rich shales in the Beibuwan Basin, South China Sea. Marine and Petroleum Geology 48, 77-89.

Hu, Z.C., Zhang, W., Liu, Y.S., Gao, S., Li, M., Zong, K.Q., Chen, H. H., Hu, S. H., 2015. “Wave” signal smoothing and mercury removing device for laser ablation quadrupole and multiple collector ICP-MS analysis: application to lead isotope analysis. Analytical Chemistry, 87, 1152–1157.

Jahn, B.M., Zhou, X.H., Li, J.L., 1990. Formation and tectonic evolution of southeastern China and Taiwan: isotopic and geochemical constraints. Tectonophysics 183, 145–160.

Jiang, P., Qin C., Yang, X., He, J., Lu, J., Zhao, Y., Luo, B., 2018. Sedimentary architecture, distribution features and genesis of steep slope fan in Upper Liushangang Formation, Weixi’nan Sag. Earth Science (in Chinese with English abstract).

Jiang, T., Cao, L., Xie, X., Wang, Z., Li, X., Zhang, Y., Zhang, D., Sun, H., 2015. Insights from heavy minerals and zircon U–Pb ages into the middle Miocene–Pliocene provenance evolution of the Yinggehai Basin, northwestern South China Sea. Sedimentary Geology 327, 32-42.

Kruskal, J., 1964. Multidimensional scaling by optimizing goodness of fit to a nonmetric hypothesis. Psychometrika 29 (1), 1–27.

Lai, Q., Ding, L., Wang, H., Yue, Y., Cai, F., 2007. Constraining the stepwise migration of the eastern Tibetan Plateau margin by apatite fission track thermochronology. Science in China Series D: Earth Sciences 50(2), 172-183.83.

Lai, W., Hu, X.M., Garzanti, E., Sun, G.Y., Garzione, C.N., BouDagher-Fadel, M., Ma, A., 2019. Initial growth of the Northern Lhasaplano (Tibetan Plateau) in the early Late Cretaceous (92 Ma). Geological Society of America Bulletin, doi.org/10.1130/B35124.1.

Lapierre, H., Jahn, B.M., Charvet, J., Yu, Y.W., 1997. Mesozoic felsic arc magmatism and continental olivine tholeiites in Zhejiang Province and their relationship with the tectonic activity in southeastern China. Tectonophysics 274 (4), 321–338.

Lehrmann, D.J., Chaikin, D.H., Enos, P., Minzoni, M., Payne, J.L., Yu, M., Goers, A., Wood, T., Richter, P., Kelley, B.M., Li, X., Qin, Y., Liu, L., Lu, G., 2015. Patterns of basin fill in Triassic turbidites of the Nanpanjiang basin: implications for regional tectonics and impacts on carbonate-platform evolution. Basin Res. 27, 587–612.

Lei, C., Clift, P.D., Ren, J., Ogg, J., Tong, C., 2019. A rapid shift in the sediment routing system of lower-upper Oligocene strata in the Qiongdongnnan Basin (Xisha Trough), Northwest South China Sea. Marine and Petroleum Geology.

Li, C.F., Xu, X., Lin, J., Sun, Z., Zhu, J., Yao, Y., Zhao, X., Liu, Q., Kulhanek, D.K., Wang, J., Song, T., Zhao, J., Qiu, N., Guan, Y., Zhou, Z., Williams, T., Bao, R., Briais, A., Brown, E.A., Chen, Y., Clift, P.D., Colwell, F.S., Dadd, K.A., Ding, W., Almeida, I.H., Huang, X.-L., Hyun, S., Jiang, T., Koppers, A.A.P., Li, Q., Liu, C., Liu, Z., Nagai, R.H., Peleo-Alampay, A., Su, X., Tejada, M.L.G., Trinh, H.S., Yeh, Y.C., Zhang, C., Zhang, F., Zhang, G.L., 2014. Ages and magnetic structures of the South China Sea constrained by deep tow magnetic surveys and IODP Expedition 349. Geochem. Geophys. Geosyst. 15, 4958–4983.

Li, J., Zhao, G., Johnston, S.T., Dong, S., Zhang, Y., Xin, Y., Wang, W., Sun, H., Yu, Y., 2017. Permo-Triassic structural evolution of the Shiwandashan and Youjiang structural belts, South China. Journal of Structural Geology 100, 24-44.

Li, J.H., Zhang, Y.Q., Dong, S.W., Johnston, S.T., 2014. Cretaceous tectonic evolution of South China: a preliminary synthesis. Earth Sci. Rev. 134 (1), 98–136.

Li, S.Y., Currie, B.S., Rowley, D.B., Ingalls, M., 2015. Cenozoic paleoaltimetry of the SE margin of the Tibetan Plateau: Constraints on the tectonic evolution of the region. Earth and Planetary Science Letters 432, 415–424.

Li, X.H., Chen, Z.G., Liu, D.Y., Li, W.X., 2003a. Jurassic gabbro-granite-syenite suites from Southern Jiangxi Province, SE China: age, origin, and tectonic significance. International Geology Review 45(10), 898-921.

Li, X.H., 1999. U–Pb zircon ages of granites from the southern margin of the Yangtze Block: timing of Neoproterozoic Jinning: Orogeny in SE China and implications for Rodinia Assembly. Precambrian Research 97(1-2), 43-57.

Li, X.H., Li, Z.X., Zhou, H., Liu, Y., Kinny, P.D., 2002. U–Pb zircon geochronology, geochemistry and Nd isotopic study of Neoproterozoic bimodal volcanic rocks in the Kangdian Rift of South China: implications for the initial rifting of Rodinia. Precambrian Research 113(1-2), 135-154.

Li, X.H., Wei, G., Shao, L., Liu, Y., Liang, X., Jian, Z., Sun, M., Wang, P., 2003b. Geochemical and Nd isotopic variations in sediments of the South China Sea: a response to Cenozoic tectonism in SE Asia. Earth Planet. Sci. Lett. 211, 207–220.

Li, Z.X., Li, X.H., Kinny, P.D., Wang, J., Zhang, S., Zhou, H., 2003. Geochronology of Neoproterozoic syn-rift magmatism in the Yangtze Craton, South China and correlations with other continents: evidence for a mantle superplume that broke up Rodinia. Precambrian Research 122(1-4), 85-109.

Li, Z.X., Li, X.H., Chung, S.L., Lo, C.H., Xu, X., Li, W.X., 2012. Magmatic switch-on and switch-off along the South China continental margin since the Permian: transition from an Andean-type to a western pacific-type plate boundary. Tectonophysics 532-535 (3), 271–290.

Liu, A., Wu, S., Cheng, W., 2011. Tectonic subsidence history and dynamic mechanism of the Dongsha rise in the Zhujiang River Mouth Basin [in Chinese with English abstract], Acta Oceanol. Sin. 33(6), 117–124.

Liu, B., Chen, J., Lu, W., et al., 2015. Spatiotemporal characteristics of precipitation changes in the Pearl River basin, China. Theor. Appl. Climatol. 1-14.

Liu, C., Clift, P.D., Carter, A., Böning, P., Hu, Z., Sun, Z., Pahnke, K., 2017. Controls on modern erosion and the development of the Pearl River drainage in the late Paleogene. Mar. Geol. 394, 52–68.

Liu, Q., Zhu, H., Shu, Y., Zhu, X., Yang, X., Chen, L., Tan, M, Geng, M., 2016. Provenance identification and sedimentary analysis of the beach and bar systems in the Palaeogene of the Enping Sag, Pearl River Mouth Basin, South China Sea. Marine and Petroleum Geology 70, 251-272.

Liu, Y.S., Hu, Z.C., Gao, S., Günther, D., Xu, J., Gao, C.G., Chen, H.H., 2008. In situ analysis of major and trace elements of anhydrous minerals by LA-ICP-MS without applying an internal standard. Chem. Geol. 257, 34–43.

Liu, Y.S., Gao, S., Hu, Z.C., Gao, C.G., Zong, K.Q., Wang, D.B., 2010. Continental and oceanic crust recycling-induced melt-peridotite interactions in the trans-North China Orogen: U-Pb dating, Hf isotopes and trace elements in zircons of mantle xenoliths. J. Petrol. 51, 537–571.

Maruyama, S., Isozaki, Y., Kimura, G., Terabayashi, M., 1997. Paleogeographic maps of the Japanese Islands: plate tectonic synthesis from 750 Ma to the present. Island Arc 6 (1), 121–142.

Ma, X., Yang, K., Li, X., Dai, C., Zhang, H., Zhou, Q., 2016. Neoproterozoic Jiangnan Orogeny in southeast Guizhou, South China: evidence from U–Pb ages for detrital zircons from the Sibao Group and Xiajiang Group. Canadian Journal of Earth Sciences 53(3), 219-230.

Morley, C.K., 2002. A tectonic model for the Tertiary evolution of strike-slip faults and rift basins in SE Asia. Tectonophysics 347, 189–215.

Morley, C.K., 2012. Late Cretaceous–early Paleogene tectonic development of SE Asia. Earth Sci. Rev. 115 (1–2), 37–75.

Morley, C.K., 2016. Major unconformities/termination of extension events and associated surfaces in the South China Seas: Review and implications for tectonic development. J. Asian Earth Sci. 120, 62–86.

Morton, A.C., Hallsworth, C., 2007. Stability of detrital heavy minerals during burial diagenesis. In: Mange, M.A., Wright, D.T. (Eds.), Heavy Minerals in Use. Developments in Sedimentology Series vol. 58, pp. 215–245.

Murphy, M.A., Yin, A., Harrison, T.M., Dürr, S.B., Chen, Z., Ryerson, F.J., Kidd, W.S.F., Wang, X., Zhou, X., 1997. Did the Indo-Asian collision alone create the Ti¬betan plateau? Geology 25, 719–722.

Pang, X., Chen, C., Zhu, M., He, M., Shen, J., Lian, S., Wu, X., Shao, L., 2009. Baiyun movement: a significant tectonic event on Oligocene/Miocene boundary in the northern South China Sea and its regional implications. Journal of Earth Science 20(1), 49-56.

Peng, S., Jin, Z., Liu, Y., Fu, J., He, L., Cai, M., Wang, Y., 2006. Petrochemistry, chronology and tectonic setting of strong peraluminous anatectic granitoids in Yunkai Orogenic Belt, western Guangdong Province, China. J. China Univ.Geosci. 17, 1–12.

Qin, X.F., Pan, Y.M., Li, R.S., Zhou, F.S., Hu, G.A., Zhong, F., 2006. Zircon SHRIMP U–Pb geochronology of the Yunkai metamorphic complex in southeastern Guangxi, China. Geol. Bull. China 25, 553–559 (in Chinese with English abstract).

Resentini, A., Goren, L., Castelltort, S., Garzanti, E., 2017. Partitioning the sediment flux by provenance and tracing erosion patterns in Taiwan. Journal Geophysical Research - Earth Surface, 122, doi:10.1002/2016JF004026.

Roger, F., Leloup, P.H., Jolivet, M., Lacassin, R., Trinh, P.T., Brunel, M., Seward, D., 2000. Long and complex thermal history of the Song Chay metamorphic dome (northern Vietnam) by multi-system geochronology. Tectonophysics 321, 449-466.

Savva, D., Pubellier, M., Franke, D., Chamot-Rooke, N., Meresse, F., Steuer, S., Auxietre, J.L., 2014. Different expressions of rifting on the South China Sea margins. Mar. Pet. Geol. 58, 579–598.

Shao, L., Pang, X., Chen, C., Shi, H., Li, Q., Qiao, P., 2008a. Late Oligocene sedimentary environments and provenance abrupt change event in the northern South China Sea. Front. Earth Sci. China 2, 138–146.

Shao, L., Pang, X., Qiao, P., 2008b. Sedimentary filling of the Pearl River Mouth Basin and its response to the evolution of the Pearl River. Acta Seismol. Sin. 26 (2), 179.

Shao, L., Qiao, P., Zhao, M., Li, Q., Wu, M., Pang, X., Zhang, H., 2015. Depositional characteristics of the northern South China Sea in response to the evolution of the Pearl River. Geol. Soc. Lond., Spec. Publ. 429.

Shao, L., Cao, L., Pang, X., Jiang, T., Qiao, P., Zhao, M., 2016. Detrital zircon provenance of the Paleogene syn-rift sediments in the northern South China Sea. Geochem. Geophys. Geosyst. 17, 255–269.

Shao, L., Cao, L., Qiao, P., Zhang, X., Li, Q., van Hinsbergen, D. J., 2017a. Cretaceous–Eocene provenance connections between the Palawan Continental Terrane and the northern South China Sea margin. Earth and Planetary Science Letters 477, 97-107.

Shao, L., Meng, A., Li, Q., Qiao, P., Cui, Y., Cao, L., Chen, S., 2017b. Detrital zircon ages and elemental characteristics of the Eocene sequence in IODP Hole U1435A: implications for rifting and environmental changes before the opening of the South China Sea. Mar. Geol. 394, 39-51.

Shellnutt, J. G., Denyszyn, S. W., Mundil, R., 2012. Precise age determination of mafic and felsic intrusive rocks from the Permian Emeishan large igneous province (SW China). Gondwana Research 22(1), 118-126.

Shi, X., Kohn, B., Spencer, S., Guo, X., Li, Y., Yang, X., Shi, H., Gleadow, A., 2011. Cenozoic denudation history of southern Hainan Island, South China Sea: constraints from low temperature thermochronology. Tectonophysics 504(1-4), 100-115.

Shu, L.S., Zhou, X.M., 2002. Late Mesozoic tectonism of Southeast China. Geological Review 48 (3), 249–260 (in Chinese with English abstract).

Shu, L.S., Zhou, X.M., Deng, P., Wang, B., Jiang, S.Y., Yu, J.H., Zhao, X.X., 2009. Mesozoic tectonic evolution of the Southeast China Block: New insights from basin analysis. J. Asian Earth Sci. 34 (3), 376–391.

Song, M., Shu, L., Santosh, M., Li, J., 2015. Late Early Paleozoic and Early Mesozoic intracontinental orogeny in the South China Craton: geochronological and geochemical evidence. Lithos 232, 360-374.

Stevens, T., Carter, A., Watson, T.P., Vermeesch, P., Andò, S., Bird, A.F., Lu, H., Garzanti, E., Cottam, M.A.; Sevastjanova, I. 2013. Genetic linkage between the Yellow River, the Mu Us desert and the Chinese Loess Plateau. Quaternary Science Reviews, 78, 355-368.

Suggate, S. M., M. A. Cottam, R. Hall, I. Sevastjanova, M. A. Forster, L. T. White, R. A. Armstrong, A. Carter, and E. Mojares., 2014, South China continental margin signature for sandstones and granites from Palawan, Philippines, Gondwana Res. 26(2), 699–718.

Sun, W., 2016. Initiation and evolution of the South China Sea: an overview. Acta Geochim. 35(3), 215–225.

Taylor, B., Hayes, D.E., 1983. Origin and history of the South China Sea basin. Washington Dc American Geophysical Union Geophysical Monograph 27, 23–56.

Tran, T.H., Izokh, A.E., Polyakov, G.V., Borisenko, A.S., Anh, T.T., Balykin, Phuong, N.T., Rudnev, S.N., Van, V.V., Nien, B.A., 2008. Permo-Triassic magmatism and metallogeny of Northern Vietnam in relation to the Emeishan plume. Russ.Geol. Geophys. 49, 480–491.

Van Hoang, L., Wu, F., Clift, P.D., Wysocka, A., Swierczewska, A., 2009. Evaluating the evolution of the Red River systembased on in situ U–Pb dating and Hf isotope analysis of zircons. Geochemistry, Geophysics, Geosystems 10, Q11008.

Vermeesch, P., 2012. On the visualisation of detrital age distributions. Chemical Geology 312, 190-194.

Vermeesch, P., 2013. Multi-sample comparison of detrital age distributions. Chemical Geology 341, 140-146.

Vermeesch, P., 2018. Dissimilarity measures in detrital geochronology, Earth-Science Reviews 178, 310-321.

Vermeesch, P., Garzanti, E., 2015. Making geological sense of ‘Big Data’in sedimentary provenance analysis. Chemical Geology, 409, 20-27.

Vermeesch, P., Resentini, A., Garzanti, E., 2016. An R package for statistical provenance analysis. Sedimentary Geology 336, 14-25.

Vezzoli, G., Garzanti, E., Limonta, M., Andò, S., Yang, S., 2016. Erosion patterns in the Changjiang (Yangtze River) catchment revealed by bulk-sample versus single-mineral provenance budgets. Geomorphology 261, 177-192.

Von Blanckenburg, F., 2005. The control mechanisms of erosion and weathering at basin scale from cosmogenic nuclides in river sediment. Earth Planet. Sci. Lett. 237,462–479.

Walia, M., Knittel, U., Suzuki, S., Chung, S.L., Pena, R. E., Yang, T.F., 2012, No Paleozoic metamorphics in Palawan (the Philippines)? Evidence from single grain U-Pb dating of detrital zircons, J. Asian Earth Sci. 52, 134–145.

Wang, C., Liang, X.Q., Xie, Y.H., Tong, C.X., Pei, J.X., Zhou, Y., Jiang, Y., Fu, J.G., Dong, C.G., Liu, P., 2014. Provenance of Upper Miocene to Quaternary sediments in the Yinggehai-Song Hong Basin, South China Sea: Evidence from detrital zircon U-Pb ages. Marine Geology 355: 202-217.

Wang, C., Liang, X.Q., Zhou, Y., Fu, J.G., Jiang, Y., Dong, C.G., Xie, Y.H., Tong, C.X., Pei, J., Liu, P., 2015. Construction of age frequencies of provenances on the eastern side of the Yinggehai Basin: Studies of LA-ICP-MS U-Pb ages of detrital zircons from six modern rivers, western Hainan, China. Earth Sci. Front. 22, 277–289 (in Chinese with English abstract).

Wang, C. Liang, X.Q., David, A.F., Tong, C.X., Liu, P., Liang, X.R., Zhang, L., 2018. Linking source and sink: Detrital zircon provenance record of drainage systems in Vietnam and the Yinggehai–Song Hong Basin, South China Sea. GSA Bulletin 131(1-2): 191-204.

Wang, C.S., Zhao, X.X., Liu, Z.F., Lippert, P.C., Graham, S.A., Coe, R.S., Yi, H.S., Zhu, L.D., Liu, S., Li, Y.L., 2008. Constraints on the early uplift history of the Tibetan Plateau. Proceedings of the National Academy of Sciences 105(13), 4987-4992.

Wang, D., Shu, L.S., 2012. Late Mesozoic basin and range tectonics and related magmatism in Southeast China. Geosci. Front. 3 (2), 109–124.

Wang, G., Cao, K., Zhang, K., Wang, A., Liu, C., Meng, Y., Xu, Y., 2011. Spatio-temporal framework of tectonic uplift stages of the Tibetan Plateau in Cenozoic. Science China Earth Sciences 54(1), 29-44.

Wang, J-G., Hu, X., Garzanti, E., Ji, W-Q., Liu, Z-C., Liu X-C., Wu. F-Y., 2017. Early Cretaceous topographic growth of the Lhasaplano, Tibetan Plateau: constraints from the Damxung Conglomerate. Journal of Geophysical Research - Solid Earth, 122, doi:10.1002/2017JB014278.

Wang, P., 2004. Cenozoic deformation and the history of sea-land interactions in Asia. Geophysical Monograph Series 149, 1-22

Wang, X. L., Zhou, J. C., Qiu, J. S., Zhang, W. L., Liu, X. M., Zhang, G. L., 2006. LA-ICP-MS U-Pb zircon geochronology of the Neoproterozoic igneous rocks from Northern Guangxi, South China: Implications for tectonic evolution. Precambrian Research 145(1-2), 111-130.

Wang, X. L., Zhou, J. C., Griffin, W. L., Wang, R.C., Qiu, J. S., O'Reilly, S.Y., Xu, X., Liu, X. M., Zhang, G. L., 2007. Detrital zircon geochronology of Precambrian basement sequences in the Jiangnan orogen: dating the assembly of the Yangtze and Cathaysia blocks. Precambrian Res. 159 (1–2), 117–131.

Wang, X. L., Zhou, J. C., Griffin, W. L., Zhao, G., Yu, J. H., Qiu, J. S., Zhang, Y. J., Xing, G. F., 2014. Geochemical zonation across a Neoproterozoic orogenic belt: isotopic evidence from granitoids and metasedimentary rocks of the Jiangnan orogen, China. Precambrian Research 242, 154-171.

Wang, Y., Wu, C., Zhang, A., Fan, W., Zhang, Y., Zhang, Y., Peng, T., Yin, C., 2012. Kwangsian and Indosinian reworking of the eastern South China Block: constraints on zircon U–Pb geochronology and metamorphism of amphibolites and granulites. Lithos 150, 227-242.

Wang, Y., Zhang, A., Fan, W., Zhao, G., Zhang, G., Zhang, Y., Zhang, F., Li, S., 2011. Kwangsian crustal anatexis within the eastern South China Block: geochemical, zircon U–Pb geochronological and Hf isotopic fingerprints from the gneissoid granites of Wugong and Wuyi-Yunkai Domains. Lithos 127, 239-260.

Wissink, G.K., Hoke, G.D., Garzione, C.N., Liu-Zeng, J., 2016. Temporal and spatial patterns of sediment routing across the southeast margin of the Tibetan Plateau: insights from detrital zircon. Tectonics 35, 2538–2563.

Xiang, H., Shao, L., Qiao, P., Zhao, M., 2011. Characteristics of heavy minerals in Pearl River sediments and their implications for provenance. Marine Geology & Quaternary Geology 31 (6), 27-35(in Chinese with English abstract).

Xie, H., D. Zhou, X. Pang, Y. Li, X. Wu, N. Qiu, P. Li, and G. Chen., 2013, Cenozoic sedimentary evolution of deepwater sags in the Pearl River Mouth Basin, northern South China Sea, Mar. Geophys. Res. 34(3–4), 159–173.

Xu, C.H., Shi, H.S., Barnes, C.G., Zhou, Z.Y., 2016. Tracing a late Mesozoic magmatic arc along the Southeast Asian margin from the granitoids drilled from the northern South China Sea. Int. Geol. Rev. 58 (1), 71–94.

Xu, J., Snedden, J.W., Stockli, D.F., Fulthorpe, C.S. and Galloway, W.E., 2017. Early Miocene continental-scale 541 sediment supply to the Gulf of Mexico Basin based on detrital zircon analysis. GSA Bulletin 129(1-2): 3-22.

Xu, X., O'Reilly, S.Y., Griffin, W.L., Wang, X., Pearson, N.J., He, Z., 2007. The crust of Cathaysia: Age, assembly and reworking of two terranes. Precambrian Res. 158, 51–78.

Xu, Y. G., Luo, Z. Y., Huang, X. L., He, B., Xiao, L., Xie, L. W., Shi, Y. R., 2008. Zircon U–Pb and Hf isotope constraints on crustal melting associated with the Emeishan mantle plume. Geochimica et Cosmochimica Acta 72(13), 3084-3104.

Xu, Y., Sun, Q., Cai, G., Yin, X., Chen, J., 2014. The U–Pb ages and Hf isotopes of detrital zircons from Hainan Island, South China: implications for sediment provenance and the crustal evolution. Environ. Earth Sci. 71, 1619–1628.

Xu, Y., Wang, C. Y., Zhao, T., 2016. Using detrital zircons from river sands to constrain major tectono-thermal events of the Cathaysia Block, SE China. Journal of Asian Earth Sciences 124, 1-13.

Yan, Q.S., Shi, X.F., Castillo, P.R., 2014. The late Mesozoic–Cenozoic tectonic evolution of the South China Sea: a petrologic perspective. J. Asian Earth Sci. 85, 178–201.

Yan, Y., Carter, A., Palk, C., Brichau, S. and Hu, X., 2011. Understanding sedimentation in the Song Hong-Yinggehai Basin, South China Sea. Geochemistry Geophysics Geosystems 12(6): Q06014.

Yang, R., Fellin, M.G., Herman, F., Willett, S.D., Wang, W., 2016. Spatial and temporal pattern of erosion in the Three Rivers Region, southeastern Tibet. Earth and Planetary Science Letters 433, 10-20.

Ye, Q., Mei, L., Shi, H., Camanni, G., Shu, Y., Wu, J., Lu, L., Deng, P., Li, G., 2018. The Late Cretaceous tectonic evolution of the South China Sea area: An overview, and new perspectives from 3D seismic reflection data. Earth-science reviews.

Yu, J.H., O'Reilly, S.Y., Wang, L., Griffin, W.L., Zhou, M.F., Zhang, M., Shu, L., 2010. Components and episodic growth of Precambrian crust in the Cathaysia Block, South China: evidence from U–Pb ages and Hf isotopes of zircons in Neoproterozoic sediments. Precambr. Res. 181, 97-114.

Zhao, L., Guo, F., Fan, W.M., Li, C.W., Qin, X.F., Li, H.X., 2010. Crustal evolution of the Shiwandashan area in South China: Zircon U–Pb–Hf isotopic records from granulite enclaves in Indo-Sinian granites. Chin. Sci. Bull. 55, 2028–2038.

Zhao, M., Shao, L., Qiao, P., 2015. Characteristics of Detrital Zircon U-Pb geochronology of the Pearl River Sands and Its Implication on Provenances. J. Tongji Univ. Nat. Sci. 43, 89–97 (in Chinese with English abstract).

Zhao, Z., Zhou, D., Liao, J., 2009. Tertiary paleogeography and depositional evolution in the Pearl River Mouth Basin of the northern South China Sea. J. Trop. Oceanogr. 28, 52–60 (in Chinese with English abstract).

Zhang, A., Wang, Y., Fan, W., Zhang, Y., Yang, J., 2012. Earliest Neoproterozoic (ca.1.0 Ga) arc-back-arc-basin nature along the northern Yunkai Domain of the Cathaysia Block: geochronological and geochemical evidence from the metabasite. Precambr. Res. 220-221, 217-233.

Zhang, J.Y., Sun, Z., Zhang, Y.F., Li, F.C., 2016. Mesozoic deformation in the Chaoshan Depression of the Pearl River Mouth Basin, northern South China Sea. Mar. Geophys. Res. 1–14.

Zhang, Q., Xiao, M., Singh, V.P., Li, J., 2012. Regionalization and spatial changing properties of droughts across the Pearl River basin, China. J. Hydrol. 472-473, 355–366.

Zheng, H., Clift, P.D., Wang, P., Tada, R., Jia, J., He, M., Jourdan, F., 2013. Pre-Miocene birth of the Yangtze River. Proceedings of the National Academy of Sciences 110(19), 7556-7561.

Zhong, L., Li, G., Yan, W., Xia, B., Feng, Y., Miao, L., Zhao, J., 2017. Using zircon U–Pb ages to constrain the provenance and transport of heavy minerals within the northwestern shelf of the South China Sea. Journal of Asian Earth Sciences 134, 176-190.

Zhou, X.M., Li, W.X., 2000. Origin of late Mesozoic igneous rocks in southeastern China: implications for lithosphere subduction and underplating of mafic magmas. Tectonophysics 326 (3), 269–287.

Zhou, M. F., Yan, D. P., Kennedy, A. K., Li, Y., Ding, J., 2002. SHRIMP U–Pb zircon geochronological and geochemical evidence for Neoproterozoic arc-magmatism along the western margin of the Yangtze Block, South China. Earth and Planetary Science Letters 196(1-2), 51-67.

Zhou, X.M., Sun, T., Shen, W.Z., Shu, L.S., Niu, Y.L., 2006. Petrogenesis of Mesozoic granitoids and volcanic rocks in South China: a response to tectonic evolution. Episodes 29 (1), 26–33.

Zong, K.Q., Klemd, R., Yuan, Y., He, Z.Y., Guo, J.L., Shi, X.L., Liu, Y.S., Hu, Z.C., Zhang, Z.M., 2017. The assembly of Rodinia: the correlation of early Neoproterozoic (ca. 900 ma) high-grade metamorphism and continental arc formation in the southern Beishan Orogen, southern central Asian Orogenic Belt (CAOB). Precambrian Res. 290, 32–48.

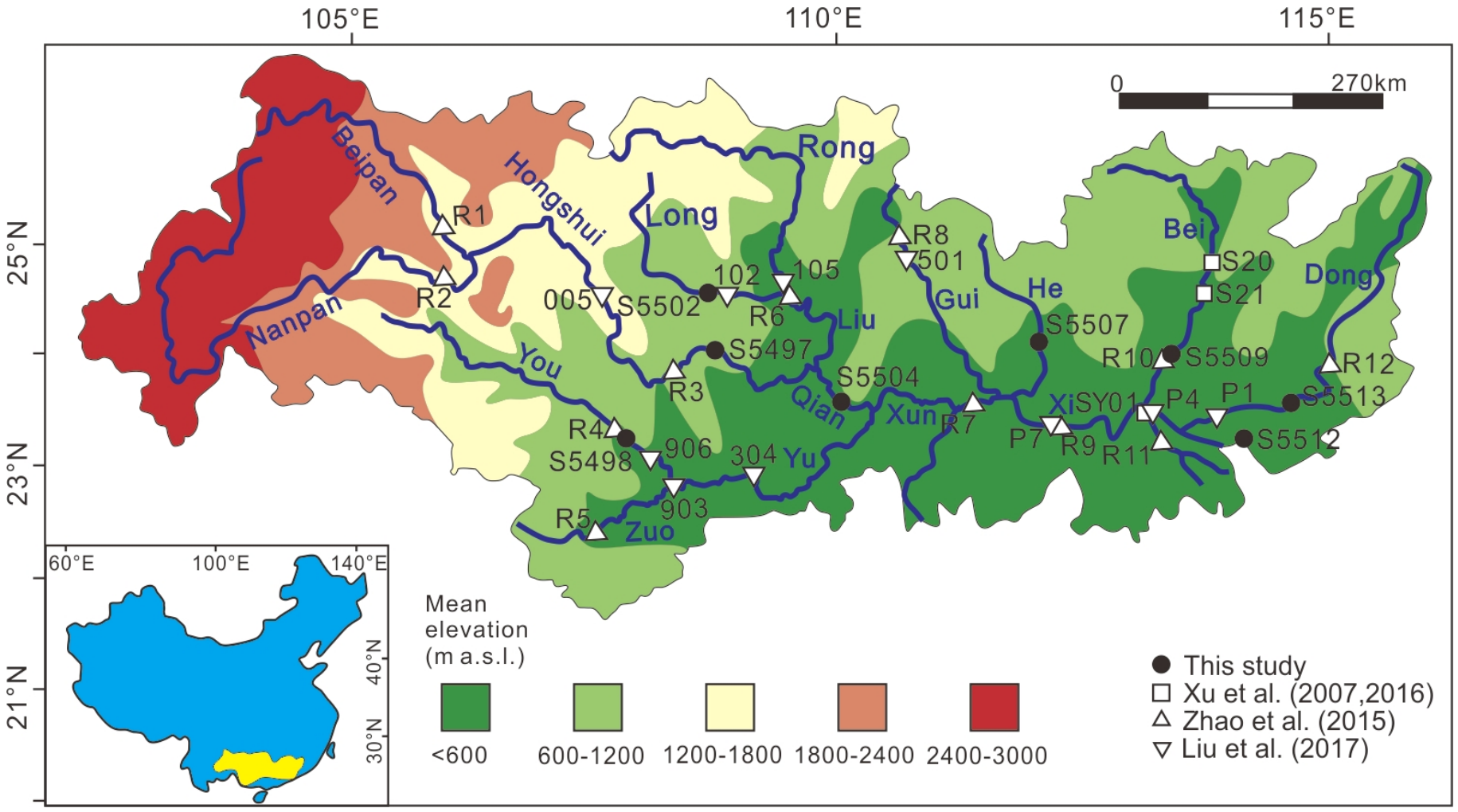
105°E
110°E
115°E
25°N
23°N
21°N
0
270km
Beipan
Hongshui
Long
Rong
Nanpan
You
Liu
Gui
He
Bei
Dong
Qian
Xun
Yu
Zuo
R1
R2
R3
R4
R5
R6
R7
R8
R9
R10
R11
R12
102
105
005
S5502
S5497
S5504
501
S5507
S20
S21
S5509
S5513
S5512
XiSY01
P4
P1
P7
906
304
903
S5498
60°E
100°E
140°E
40°N
30°N
Mean
elevation
(m a.s.l.)
<600
600-1200
1200-1800
1800-2400
2400-3000
This study
Xu et al. (2007,2016)
Zhao et al. (2015)
Liu et al. (2017)

Figure 1

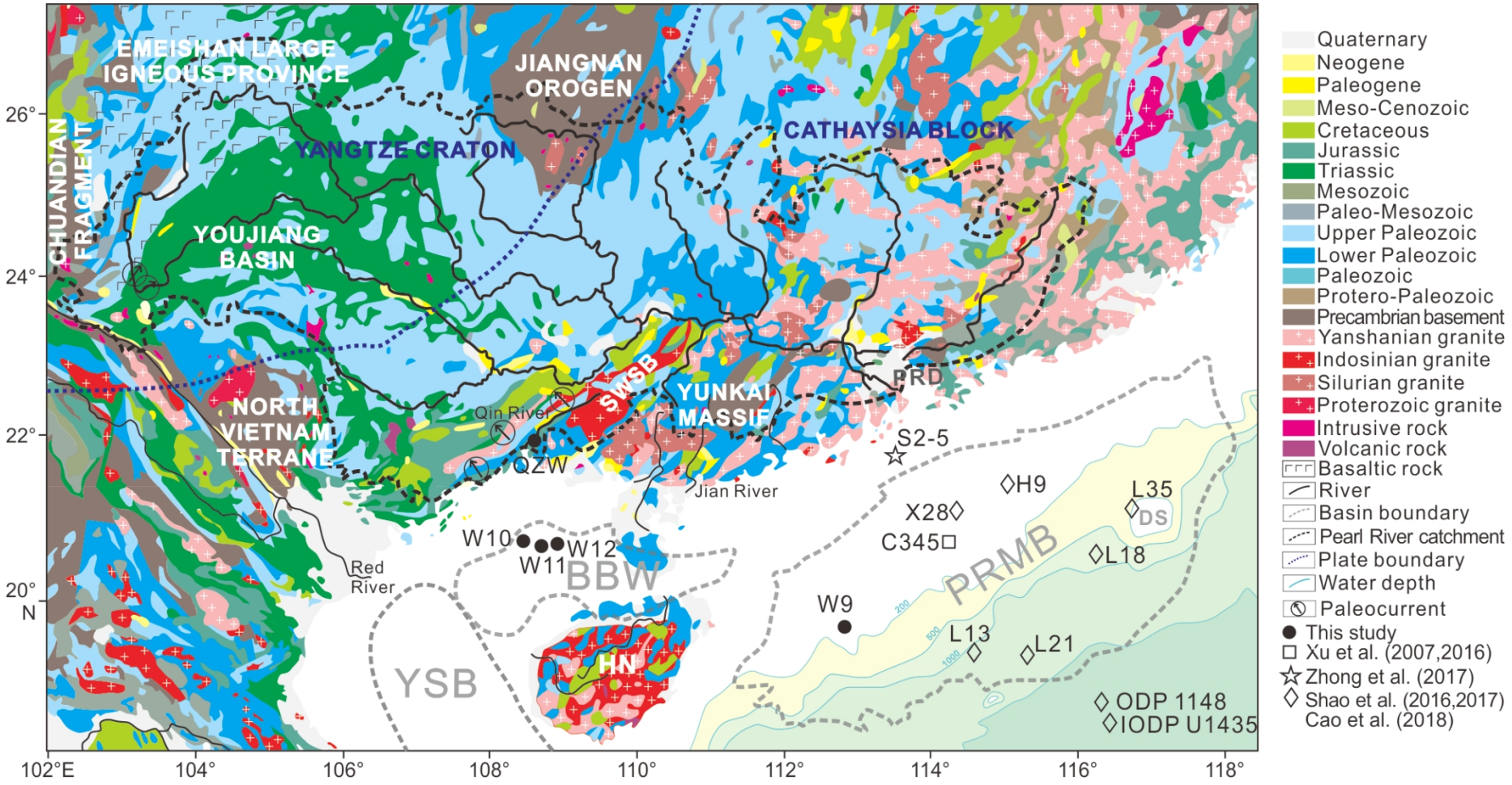
EMEISHAN LARGE IGNEOUS PROVINCE
JIANGNAN OROGEN
CATHAYSIA BLOCK
YANGTZE CRATON
CHUANDIAN FRAGMENT
YOUJIANG BASIN
NORTH VIETNAM TERRANE
SWSB
YUNKAI MASSIF
PRD
Qin River
QZW
Jian River
Red River
W10
W11
W12
BBW
YSB
HN
S2-5
H9
L35
DS
X28
C345
L18
PRMB
W9
L13
L21
ODP 1148
IODP U1435
26°
24°
22°
20°
N
102°E
104°
106°
108°
110°
112°
114°
116°
118°
Quaternary
Neogene
Paleogene
Meso-Cenozoic
Cretaceous
Jurassic
Triassic
Mesozoic
Paleo-Mesozoic
Upper Paleozoic
Lower Paleozoic
Paleozoic
Protero-Paleozoic
Precambrian basement
Yanshanian granite
Indosinian granite
Silurian granite
Proterozoic granite
Intrusive rock
Volcanic rock
Basaltic rock
River
Basin boundary
Pearl River catchment
Plate boundary
Water depth
Paleocurrent
This study
Xu et al. (2007,2016)
Zhong et al. (2017)
Shao et al. (2016,2017)
Cao et al. (2018)

Figure 2

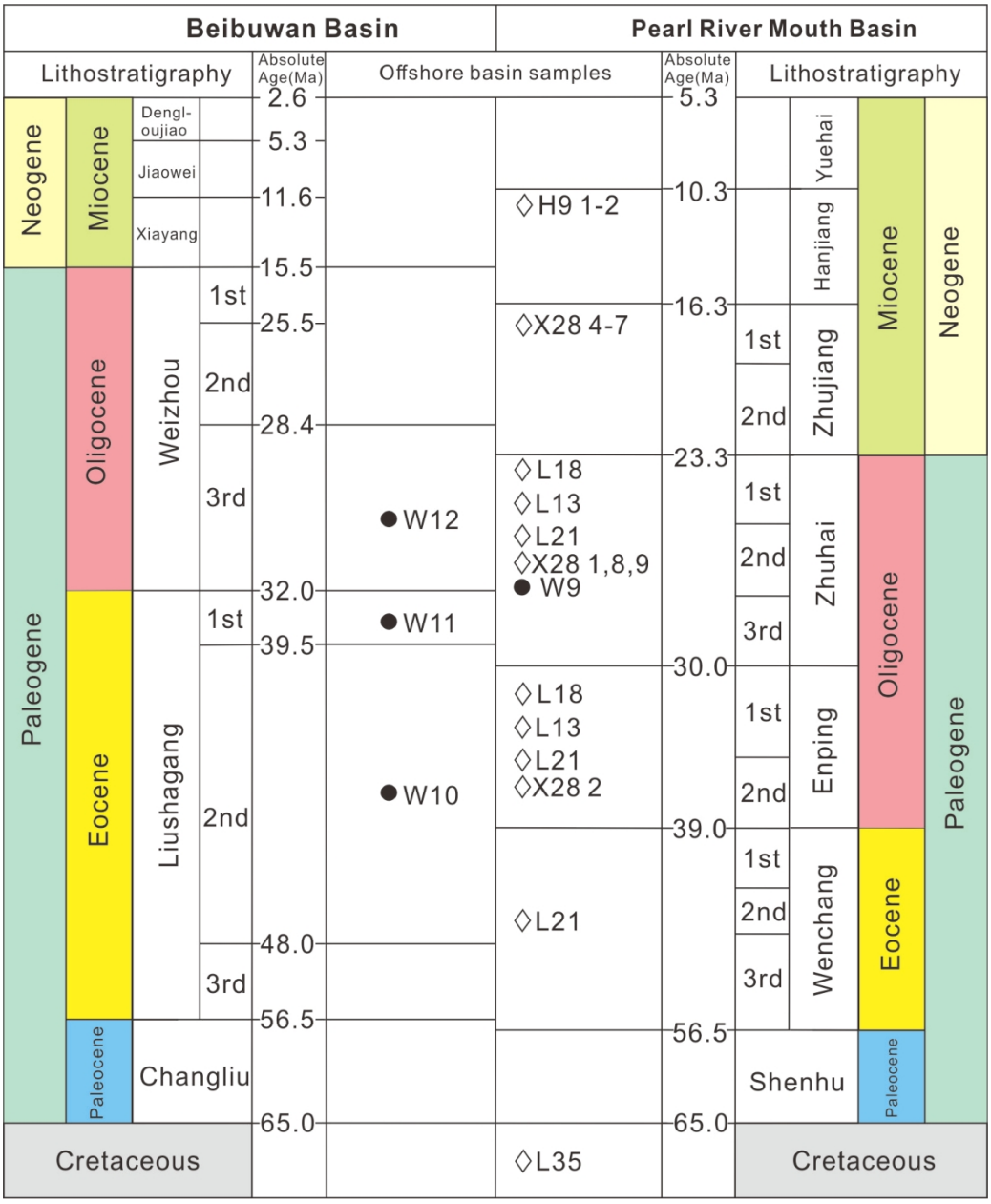
Beibuwan Basin
Pearl River Mouth Basin
Lithostratigraphy
Absolute Age(Ma)
Offshore basin samples
Absolute Age(Ma)
Lithostratigraphy
Neogene
Miocene
Dengl-oujiao
Jiaowei
Xiayang
2.6
5.3
11.6
15.5
◊H9 1-2
10.3
Yuehai
Hanjiang
16.3
◊X28 4-7
1st
2nd
Zhujiang
Miocene
Neogene
Paleogene
Oligocene
Weizhou
1st
2nd
3rd
25.5
28.4
23.3
◊L18
◊L13
◊L21
◊X28 1,8,9
● W9
● W12
1st
2nd
3rd
Zhuhai
32.0
● W11
1st
39.5
30.0
◊L18
◊L13
◊L21
◊X28 2
1st
2nd
Enping
Oligocene
Eocene
Liushagang
2nd
● W10
39.0
◊L21
1st
2nd
3rd
Wenchang
Eocene
48.0
3rd
56.5
56.5
Paleocene
Changliu
Shenhu
Paleocene
65.0
65.0
Cretaceous
◊L35
Cretaceous

Figure 3

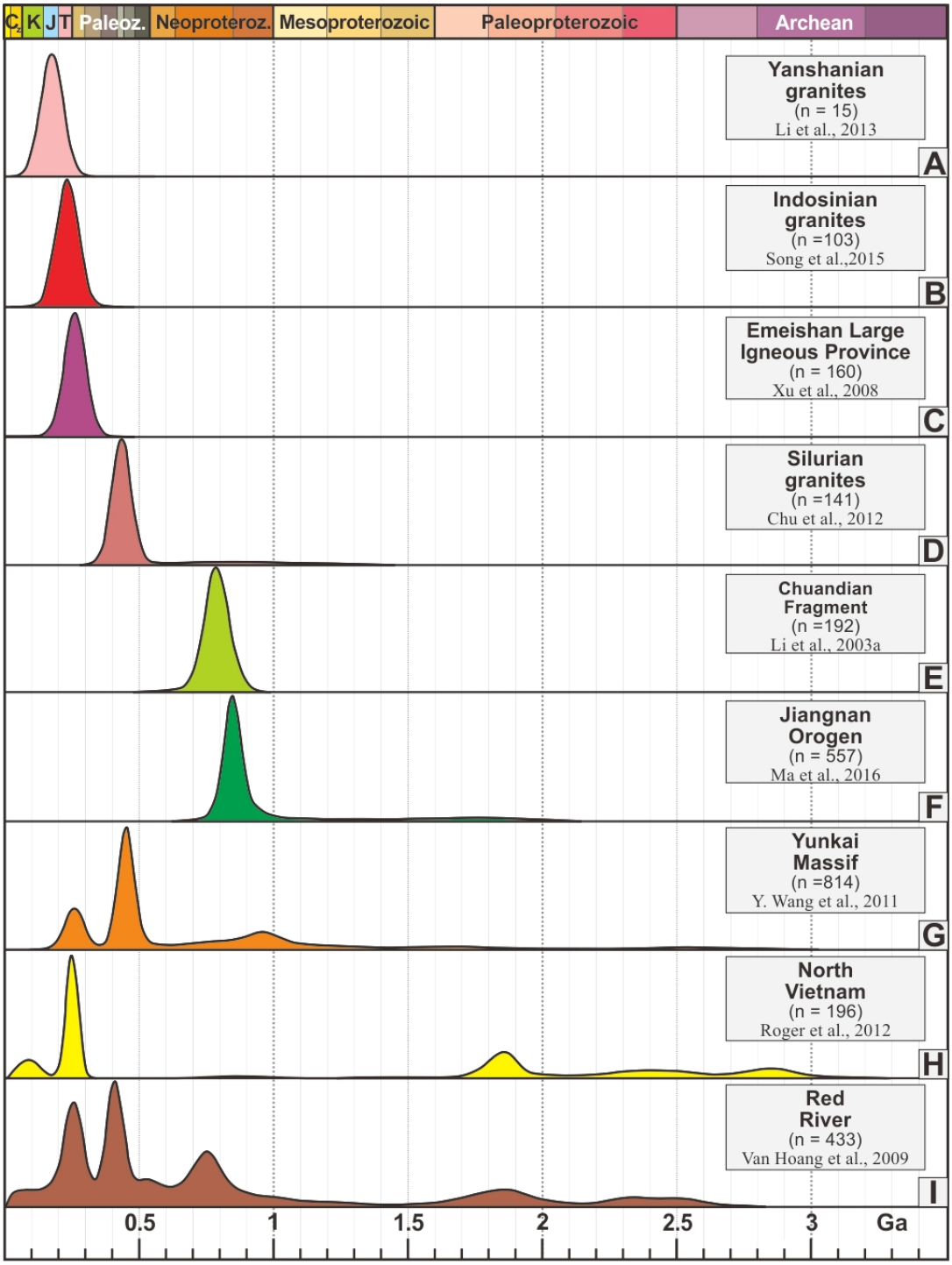
C2
K
J
T
Paleoz.
Neoproteroz.
Mesoproterozoic
Paleoproterozoic
Archean
Yanshanian granites
(n = 15)
Li et al., 2013
A
Indosinian granites
(n =103)
Song et al.,2015
B
Emeishan Large Igneous Province
(n = 160)
Xu et al., 2008
C
Silurian granites
(n =141)
Chu et al., 2012
D
Chuandian Fragment
(n =192)
Li et al., 2003a
E
Jiangnan Orogen
(n = 557)
Ma et al., 2016
F
Yunkai Massif
(n =814)
Y. Wang et al., 2011
G
North Vietnam
(n = 196)
Roger et al., 2012
H
Red River
(n = 433)
Van Hoang et al., 2009
I
0.5
1
1.5
2
2.5
3
Ga

Figure 4

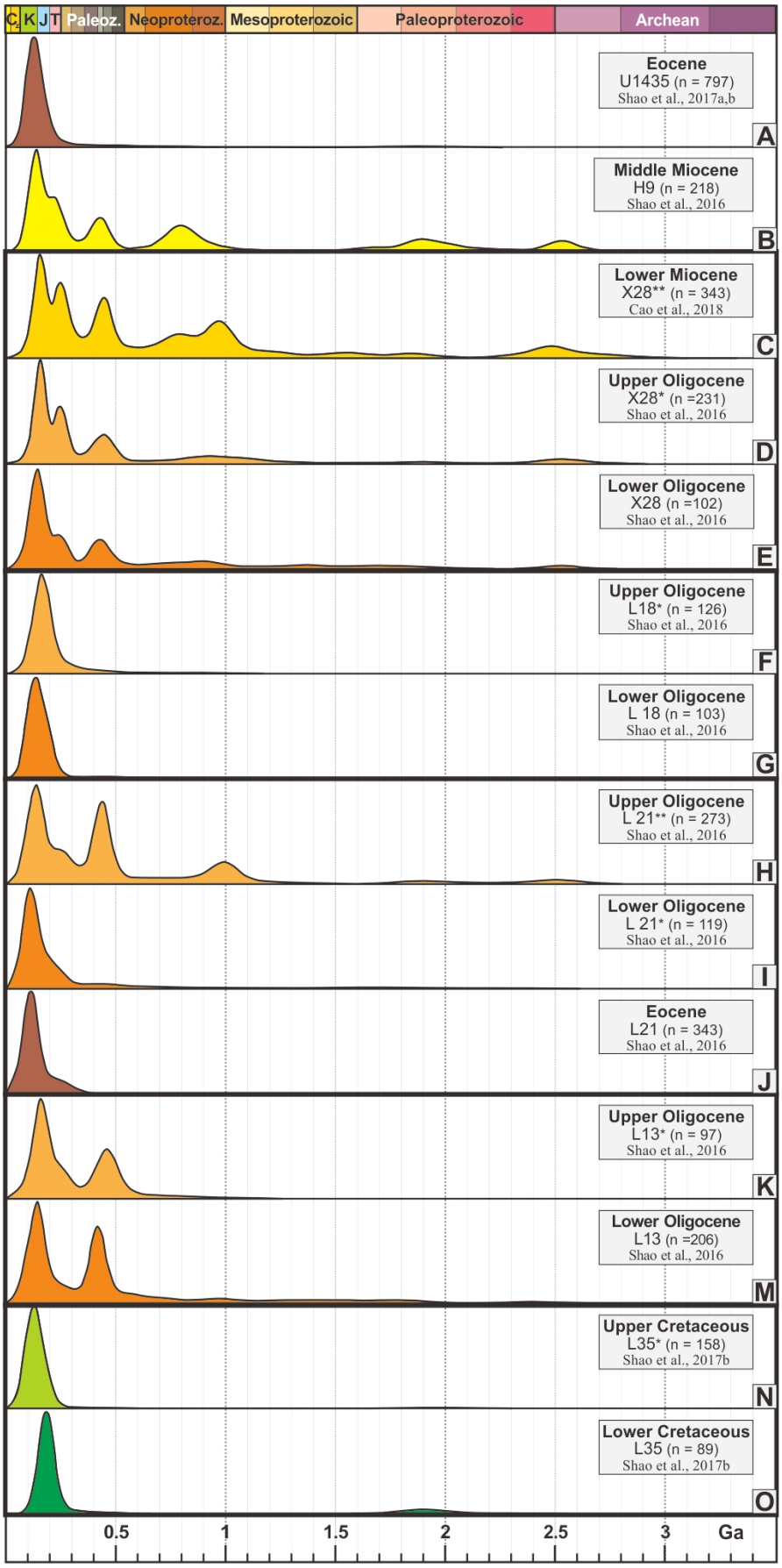
Cz
K
J
T
Paleoz.
Neoproterozoic
Mesoproterozoic
Paleoproterozoic
Archean
Eocene
U1435 (n = 797)
Shao et al., 2017a,b
A
Middle Miocene
H9 (n = 218)
Shao et al., 2016
B
Lower Miocene
X28** (n = 343)
Cao et al., 2018
C
Upper Oligocene
X28* (n =231)
Shao et al., 2016
D
Lower Oligocene
X28 (n =102)
Shao et al., 2016
E
Upper Oligocene
L18* (n = 126)
Shao et al., 2016
F
Lower Oligocene
L 18 (n = 103)
Shao et al., 2016
G
Upper Oligocene
L 21** (n = 273)
Shao et al., 2016
H
Lower Oligocene
L 21* (n = 119)
Shao et al., 2016
I
Eocene
L21 (n = 343)
Shao et al., 2016
J
Upper Oligocene
L13* (n = 97)
Shao et al., 2016
K
Lower Oligocene
L13 (n =206)
Shao et al., 2016
M
Upper Cretaceous
L35* (n = 158)
Shao et al., 2017b
N
Lower Cretaceous
L35 (n = 89)
Shao et al., 2017b
O
0.5
1
1.5
2
2.5
3
Ga

Figure 5

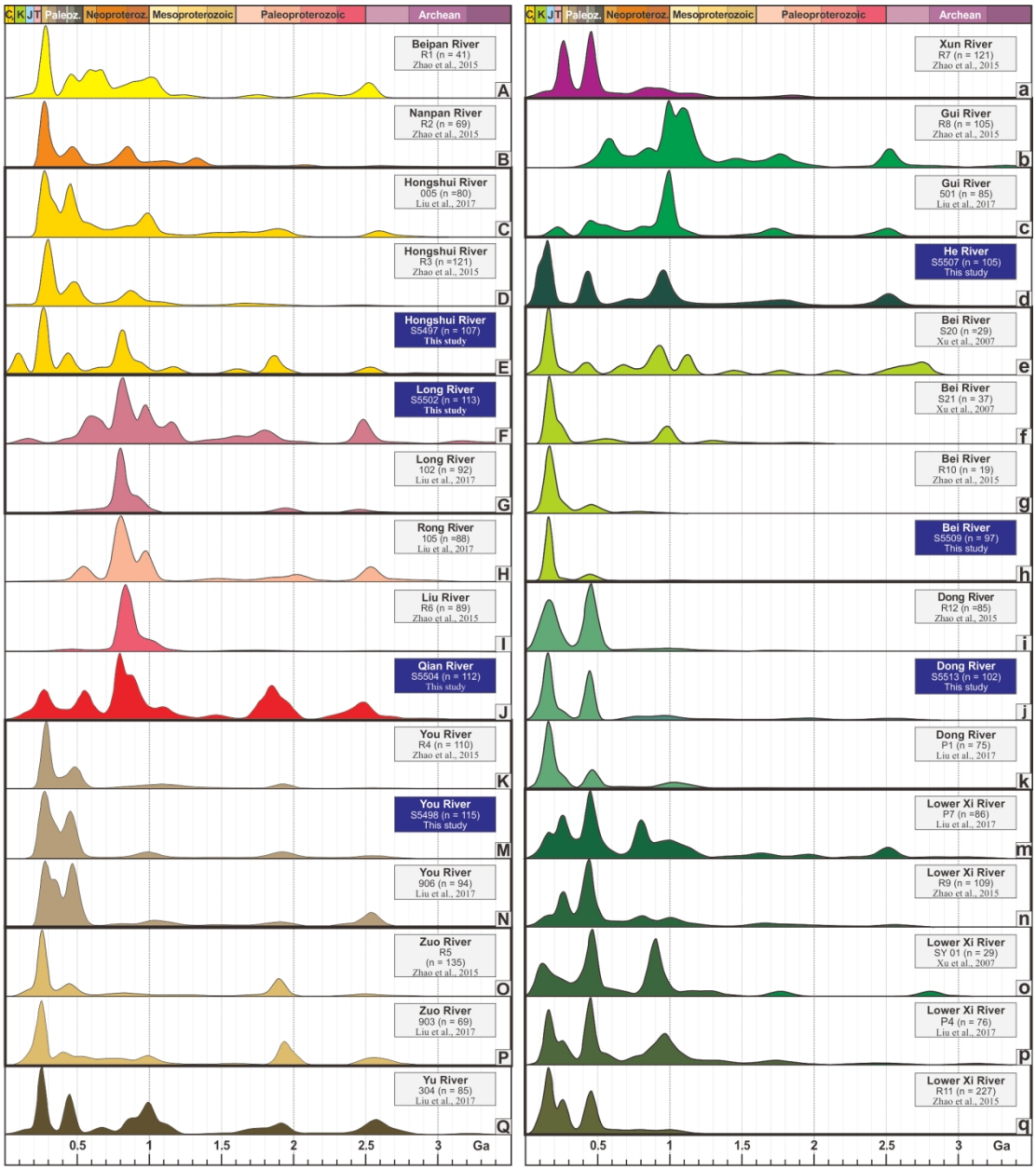

Figure 6

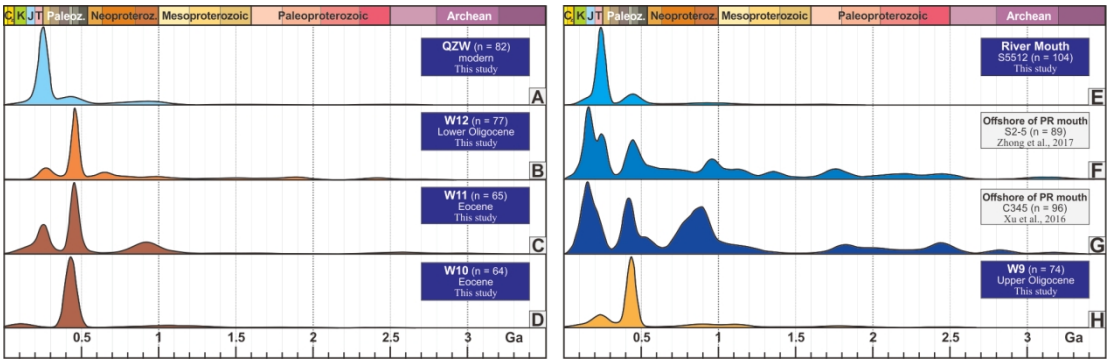

Figure 7

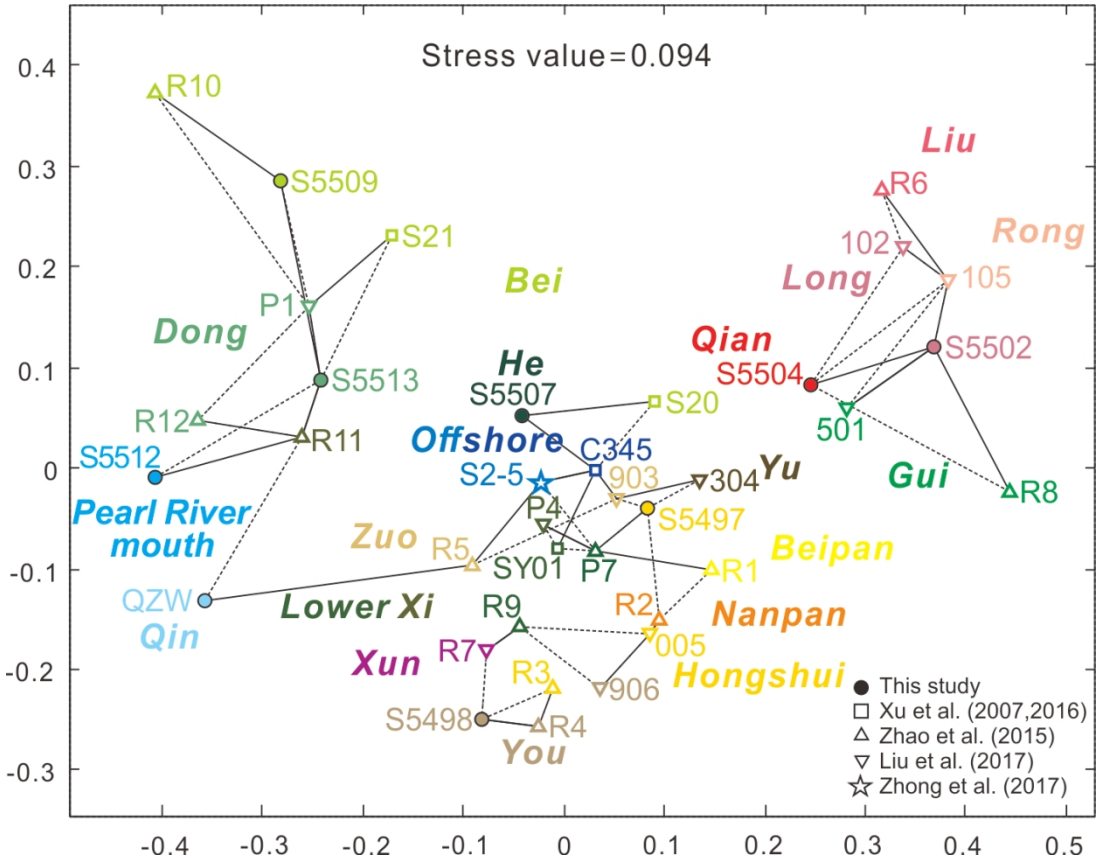
Stress value=0.094
R10
S5509
S21
P1
S5513
R12
R11
S5512
QZW
R5
SY01
P7
P4
S5497
R1
R9
R2
R7
005
R3
906
S5498
R4
S5507
S20
C345
S2-5
903
304
S5504
501
S5502
R6
102
105
R8
Liu
Rong
Long
Bei
Dong
He
Offshore
Qian
Yu
Gui
Pearl River mouth
Zuo
Beipan
Lower Xi
Nanpan
Qin
Xun
Hongshui
You
This study
Xu et al. (2007,2016)
Zhao et al. (2015)
Liu et al. (2017)
Zhong et al. (2017)
0.4
0.3
0.2
0.1
0
-0.1
-0.2
-0.3
-0.4
-0.3
-0.2
-0.1
0
0.1
0.2
0.3
0.4
0.5

Figure 8

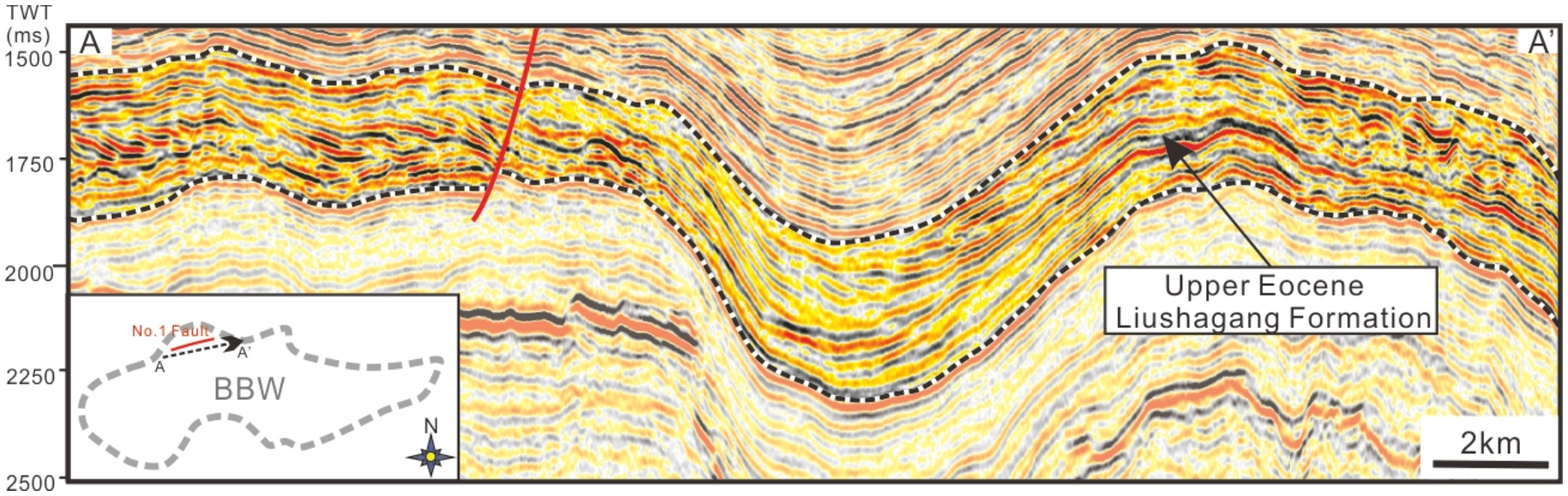
TWT
(ms)
1500
1750
2000
2250
2500
A
A'
Upper Eocene
Liushagang Formation
No.1 Fault
A
A'
BBW
N
2km

Figure 9

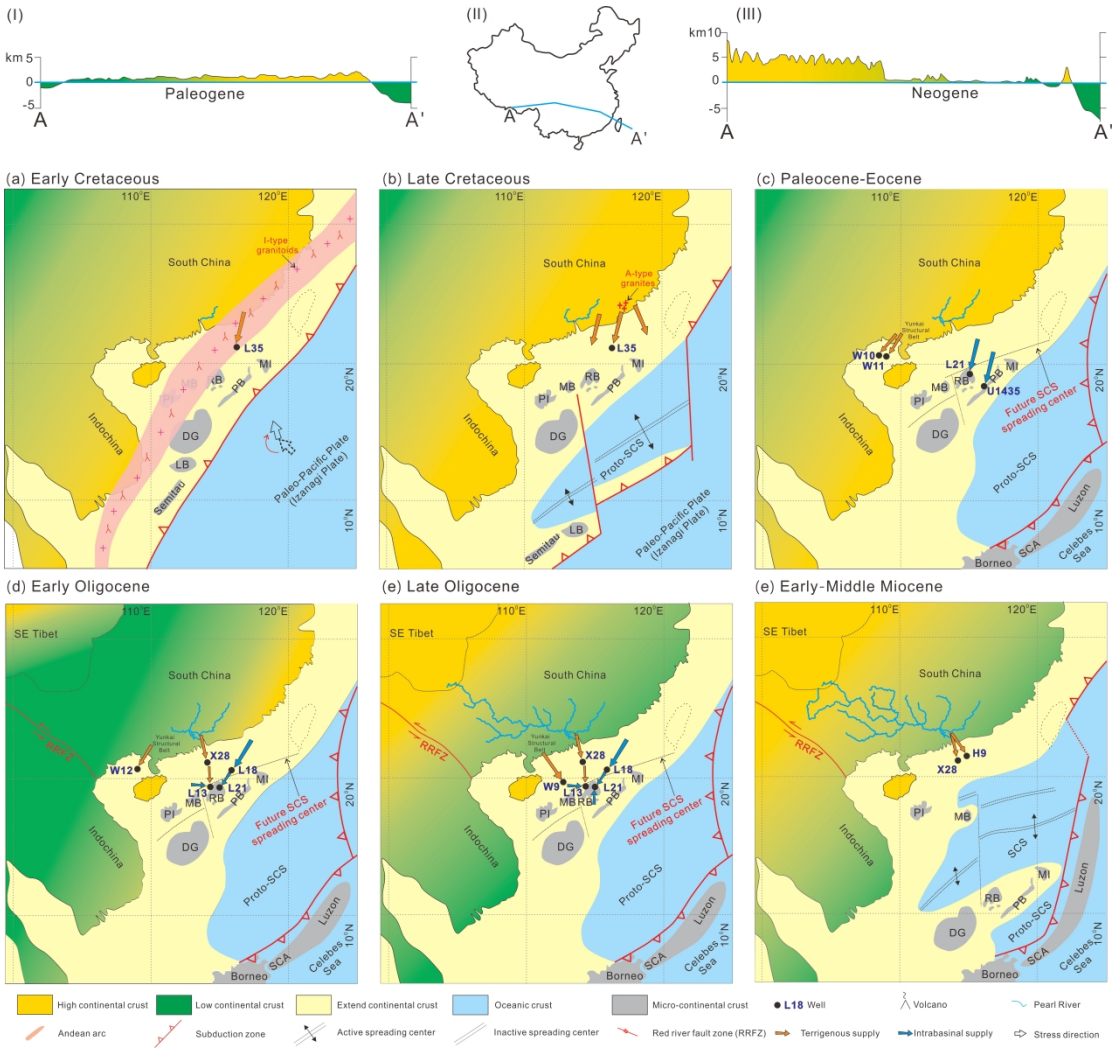
(I)
km 5
0
-5
Paleogene
A
A'
(II)
A
A'
(III)
km10
5
0
-5
Neogene
A
A'
(a) Early Cretaceous
(b) Late Cretaceous
(c) Paleocene-Eocene
(d) Early Oligocene
(e) Late Oligocene
(e) Early-Middle Miocene
110°E
120°E
20°N
10°N
South China
SE Tibet
Indochina
Borneo
Luzon
Celebes Sea
SCA
I-type granitoids
A-type granites
Yunkai Structural Belt
RRFZ
Future SCS spreading center
Proto-SCS
Paleo-Pacific Plate (Izanagi Plate)
Semisu
DG
LB
MB
RB
PB
PI
MI
SCS
L35
W10
W11
L21
U1435
X28
W12
L18
L13
W9
H9
High continental crust
Low continental crust
Extend continental crust
Oceanic crust
Micro-continental crust
L18 Well
Volcano
Pearl River
Andean arc
Subduction zone
Active spreading center
Inactive spreading center
Red river fault zone (RRFZ)
Terrigenous supply
Intrabasinal supply
Stress direction

Figure 10